General Disclaimer

One or more of the Following Statements may affect this Document

- This document has been reproduced from the best copy furnished by the organizational source. It is being released in the interest of making available as much information as possible.

- This document may contain data, which exceeds the sheet parameters. It was furnished in this condition by the organizational source and is the best copy available.

- This document may contain tone-on-tone or color graphs, charts and/or pictures, which have been reproduced in black and white.

- This document is paginated as submitted by the original source.

- Portions of this document are not fully legible due to the historical nature of some of the material. However, it is the best reproduction available from the original submission.

NASA

Technical Memorandum 86150

POLAR RAIN: SOLAR CORONAL ELECTRONS IN THE EARTH'S MAGNETOSPHERE

D.H. Fairfield

J.D. Scudder

DECEMBER 1984

National Aeronautics and
Space Administration

Goddard Space Flight Center
Greenbelt, Maryland 20771

Polar Rain: Solar Coronal Electrons in the Earth's Magnetosphere

D. H. Fairfield and J. D. Scudder

Laboratory for Extraterrestrial Physics

NASA/Goddard Space Flight Center, Greenbelt, Maryland 20771

Submitted to J. Geophysical Research

August 28, 1984

Abstract

ISEE-1 low energy electron measurements have revealed the frequent presence of field-aligned fluxes of few hundred eV electrons in the geomagnetic tail lobes. In the northern tail lobe these electrons are most prominent when the interplanetary magnetic field is directed away from the sun. This characteristic helps identify the electrons as polar rain electrons that are usually identified by their uniform precipitation pattern over the earth's polar caps. Although tail lobe electrons have been seen previously at high altitudes, the ISEE data provide the first demonstration of their field aligned nature and this characteristic places a stringent constraint on their origin. By mapping the tail lobe velocity distribution function into the solar wind, we have confirmed previous suggestions that the polar rain is indeed of solar wind origin and is due to the access of electrons to the magnetotail lobe. More specifically, however, it is demonstrated that the more energetic component of the polar rain is composed of electrons from the solar wind "strahl" - a field-aligned component of the solar wind which is difficult to measure but which is thought to be caused by the collisionless transit of hundred eV electrons from the inner solar corona to 1 AU. The preferential entry of the strahl into that polar cap most directly connected magnetically to the sun explains a known north-south asymmetry in polar rain intensity. Furthermore, it is suggested that cases of higher energy polar rain that have been thought to require a magnetospheric field aligned acceleration mechanism are more likely due to an enhanced intensity of the solar wind strahl caused by easier access of solar corona electrons to 1 AU and the polar caps. This idea is supported by the observation that previously reported cases of intense polar rain are invariably associated with tenuous or high speed solar wind that is expected to produce enhanced strahls. It is

shown how polar rain measurements may provide a good measure of (1) the temperature and the state of statistical equilibrium in the solar corona, and (2) the degree to which interplanetary field lines connect with those of the earth.

1. Introduction

Although magnetospheric field lines poleward of the auroral zone have long been known for their dearth of plasma, sensitive measurements in recent years have revealed the presence of low energy electrons on these field lines. These few hundred eV electrons frequently precipitate rather uniformly over the entire polar cap and have been termed the "polar rain" by Winningham and Heikkila [1974]. They exist on field lines that lead to the lobes of the magnetic tail and indeed measurements in the northern lobe [Yeager and Frank, 1976] have revealed the presence of these electrons at $\sim$3-7R_e.

An interesting characteristic of these high latitude electrons is that their access to the magnetosphere is regulated by the polarity of the interplanetary magnetic field (IMF) sector structure. In the northern hemisphere of the magnetosphere, 300-500 eV electrons were found to be much more intense when the interplanetary field was pointing away from the sun (away sectors) [Yeager and Frank, 1976]. At low altitudes over the polar caps a north-south asymmetry was often detected with the north to south polar cap intensity ratios tending to be greater or less than unity depending on whether the earth was immersed in an away or toward sector [Fennell et al., 1975; Meng and Kroehl, 1977; Mizera and Fennell, 1978]. It has also been noted that spectra of these electrons are similar to the cusp [Winningham and Heikkila,

1974] and the magnetosheath [Yeager and Frank, 1976]. Fennell et al. [1975] presented one example of rather good agreement among nearly simultaneous measurements in the tail lobe, over the polar cap, and in interplanetary space.

The above facts led to the suggestion that low energy electrons have unimpeded access to the polar cap [Winningham and Heikkila, 1974; Fennell et al., 1975] in the same manner as energetic solar flare electrons [e.g. Paulikas, 1974]. This concept is illustrated in Figure 1 which shows field lines from one polar cap connecting to interplanetary field lines leading directly back to the sun while field lines from the other hemisphere connect to field lines continuing far out into the solar system. Which polar cap connects most directly to the sun is controlled by the interplanetary sector structure. A directed flux of electrons moving along field lines and coming from the sun (open arrows) would preferentially be directed into one polar cap or the other in order to produce the north-south asymmetry. The interplanetary heat flux was suggested as the source of this asymmetry [Fennell et al., 1975], but detailed comparisons of interplanetary distributions functions and magnetospheric measurements have not been carried out.

Other measurements have also shown that the intensities over the polar cap at any given time often exhibit large scale nonuniformities. Meng et al. 1977 have presented evidence for a dawn-dusk intensity gradient that depends on the IMF. When the interplanetary B_y is positive (negative) the northern hemisphere fluxes tend to be higher near dawn (dusk). The situation reverses in the southern hemisphere. These variations are similar to IMF dependence of the polar cap electric field [Heppner, 1972; Burke et al., 1979] with regions of strong E corresponding to regions of high precipitating flux.

Corresponding dawn-dusk variations of electron intensity were not seen in the tail [Yeager and Frank, 1976] but this may be due to the inability of a more distant spacecraft to sample different spatial regions in times that are short compared to the variability of polar rain. Very recently Gussenhoven et al. [1984] have discovered a day to night decrease (increase) in integral flux (average energy) in low altitude measurements of the polar rain.

In their original study of ISIS traversals of the polar cap, Winningham and Heikkila [1974] defined two additional classes of somewhat more intense and energetic polar precipitation. "Polar showers" were narrow structures embedded within broader polar rain regions which undoubtedly correspond to polar cap auroral arcs [see also Hardy, 1984]. These structures will not be of interest here. "Polar squalls" were broader regions of enhanced keV electron precipitation associated with magnetically disturbed intervals. Low energy photoelectrons emitted from the polar cap were often seen returning to low altitudes within these squall regions whereas within polar rain regions these particles were usually moving outward and presumably escaping along open field lines [Winningham and Heikkila, 1974; Winningham and Gurgiolo, 1982]. These returning photoelectrons led to the suggestion that parallel electric fields over the polar cap were involved both in accelerating the more energetic squall electrons and causing photoelectrons to return to low altitudes. Heppner et al. [1981] have presented further evidence for such parallel electric fields.

Foster and Burrows [1976] also studied intervals of uniform keV-type polar precipitation which were similar to polar squalls except that each of their two events covered practically the whole polar cap and each occurred during the quiet interval following a storm. Meng and Kroehl [1977] presented two similar events. Foster and Burrows [1976; 1977] also suggested that these

more energetic electrons were accelerated by field aligned electric fields. This proposal was based largely on the facts that (1) the north-south asymmetry eliminated the possibility that the electrons were bouncing on closed field lines, and (2) simultaneous interplanetary measurements failed to reveal comparable fluxes that might have been entering the magnetosphere. Meng and Kroehl had no interplanetary measurements and they favored a solar origin for their intense precipitation. Comparable measurements of intense fluxes in the tail lobes have not been reported. Currently, a field aligned acceleration mechanism seems to be favored as the explanation for these more energetic polar rain-like events seen over the polar caps [Foster and Burrows, 1977; Mizera and Fennell, 1978]. The recent measurements (Gussenhoven et al., 1984] even suggest a role for the magnetosphere in modulating normal polar rain.

In the following sections we describe ISEE-1 measurements of anisotropic, field-aligned, tail lobe electrons whose occurrence characteristics identify them as the tail lobe component of the electron distribution function that precipitates as polar rain. We then examine the question of solar wind origin of the polar rain using contemporary knowledge of anisotropic solar wind distribution functions that was not available at the time of earlier magnetospheric measurements. By mapping these distribution functions along field lines between the solar wind and the tail lobe, we quantitatively demonstrate that the polar rain is indeed of solar wind origin with the north-south asymmetry due to the previously unknown anisotropic component of the solar wind - the strahl. We review information on the solar origin of the strahl and reinvestigate the question of whether intense polar rain events could be of solar origin rather than due to magnetospheric acceleration. We conclude that the limited information on these intense events is consistent

with this solar wind hypothesis although the possibility of further magnetospheric acceleration remains a possibility. The solar origin of the polar rain has various implications for both solar and magnetospheric physics which are discussed.

2. Instrument and Data Reduction

The ISEE 1 electron spectrometer was designed primarily to provide high time resolution, three dimensional measurements in the relatively dense plasma at the magnetopause and beyond [Ogilvie et al., 1978]. To achieve this goal six individual sensors with 8.5° x 11° viewing angles were mounted to form two mirror imaged triaxial spectrometers, each with three mutually orthogonal fields of view. The six sensors are simultaneously sampled at logarithmically spaced energies extending over a range which is set to either 11 eV to 2.06 keV (Mode 2) or 109 eV to 7.28 keV (Mode 3) when the spacecraft is in the magnetotail. Each energy sweep takes 0.5 s or 1/6 of a 3 second spacecraft spin. As the spacecraft spins the individual sensors, which make angles of ±16.2, ±31.7, and ±53.5 degrees with the spacecraft equatorial plane, sweep out 6 spatial bands on the unit sphere while they are each undergoing 6 energy sweeps. Thus each energy is sampled 6 times by each of 6 detectors giving 36 widely separated points on the unit sphere, half of which are located diametrically opposite to another simultaneously sampled point. In the high (low) bit rate mode every third (sixth) 3 s spin is sampled giving complete data sets every 9 or 18 s. These measurements yield 36 point determinations of the pitch angle variation on every spin when combined with the 1 minute $\vec{B}$ data from the experiment of C. T. Russell obtained via the ISEE data pool tapes.

In the course of calculating moments of the electron distribution function, f, the value of f is determined for each of the 36 measurement directions at each energy. To obtain a rough measure of the electron isotropy, at each energy we calculate an average $f_\perp$ for all measurements with pitch angles 90° ±30° and an average $f_\parallel$ for all the remaining f values having pitch angles within 60° of the parallel or anti-parallel field direction. Plots of $f_\parallel$ and $f_\perp$ versus time have proven useful in identifying magnetotail anisotropies.

3. Polar Rain in the Tail Lobe

Initial scans of ISEE 1 electron data in the magnetotail revealed the presence of occasional intervals of persistent anisotropic field aligned fluxes in the tail lobes with energies typically ranging up to a few hundred eV. An example of such anisotropic fluxes is shown in Figure 2 where the measured log of the distribution function f (irregular solid lines) is plotted versus pitch angle. Each tic mark on the ordinate represents one decade in f and the adjacent energies have been offset 1.25 decades to prevent overcrowding. Fluxes are low, as is characteristic of the tail lobes, so instrumental counts have been averaged over 30 consecutive spins (five minutes). Only background counts are detected for pitch angles near 90° for energies above 180 eV, but the counting rates rise to several tens of counts per spin above background for the lowest and highest pitch angles. One count levels are indicated by dashed lines. Note that the logarithimic scale of f tends to deemphasize this more dramatic increase in the counting rate near the field direction. The fluxes are approximately symmetric parallel and anti-parallel to the field direction and they are only detected within about

30° of the field direction. Another important characteristic illustrated by Figure 2 is the energy dependence of the anisotropy; the lower energy electrons are invariably more isotropic than those at higher energies.

To investigate the persistence of these anisotropic electron fluxes we utilize plots of the average $f_{\parallel}$ and $f_{\perp}$ as defined above. Since $f_{\parallel}$ is an average of all measurements within 60° of the field direction, it has a magnitude that is substantially diminished relative to the actual f value near 0° or 180° pitch angle. In spite of this fact, these average $f_{\parallel}$ and $f_{\perp}$ values serve as useful indicators of the anisotropy. An example of such data covering six hours on April 18, 1978 is shown in Figure 3. The lines representing $f_{\parallel}$ and dots representing $f_{\perp}$ are plotted on a logarithimic scale; every third point is omitted to prevent overcrowding and successive energies are offset by one decade. The example of Figure 2 comes from this interval and the separation of the traces in Figure 3 can be seen at the energies where the anisotropy is apparent in Figure 2. The fluxes are relatively steady on this scale of hours until the plasma sheet (more intense energetic electrons) is approached shortly after 0700.

The observed characteristics of these lobe electrons suggest that they may be polar rain electrons. The fact that anisotropic lobe electrons are seen in the northern tail lobe on some days but not on other days is consistent with the preferred-polar cap entry process. Their steady nature when present is similar to low altitude observations and their energy range is similar to polar rain. Although previous measurements on tail lobe field lines did not reveal any pitch angle anisotropy [Yeager and Frank, 1976], there appear to be good reasons for this. These workers were using a wider

angle detector that summed counts over 55° of azimuthal spin. They were also measuring primarily at 3-7 R_e where the anisotropy would be less pronounced than in the deeper tail (see discussion below). At these altitudes the field direction was also probably not often directed into their viewing angle.

To strengthen the evidence that anisotropic lobe electrons are indeed polar rain electrons, a statistical survey was undertaken of tail lobe hourly averages. Various quantities were averaged including $f_{\parallel}$, $f_{\perp}$ and the ratio of their hourly averages. Using the electron measurements along with the data pool magnetic field and occasionally the ion spectrograms of L. A. Frank, 399 hours were identified when ISEE 1 was in the tail lobe (excluding magnetopause boundary layer and plasma mantle) during the interval February 10 - June 7, 1978. During these hours the lobe electrons were investigated as a function of interplanetary sector structure or interplanetary B_y component. Of these 399 lobe hours, only 208 (52%) corresponded to hours when IMF measurements were available and only 43 of these corresponded to positive B_y when lobe electrons are expected to be present. If, however, the sector structure as determined from ground magnetograms was used [Lincoln, 1983], 351 (88%) of the hours could be associated with toward or away sectors and 89 of these hours corresponded to away sectors. Although the direct measurement is obviously more accurate when available, a comparison of the two methods confirmed the relatively high accuracy of the ground determinations and we use the latter method because of its greater completeness.

In Figure 4 we show a histogram of the parallel to perpendicular f ratios for the two sector polarities. It is important to realize that not only is $f_{\parallel}$ a lower bound on the actual maximum f at 0° pitch angle due to averaging over a range of pitch angles, but $f_{\perp}$ is an upper bound set by the instrumental threshold which is undoubtedly much higher than the actual f at 90° pitch

angle. Both effects imply that the computed ratios are lower bounds. In toward sectors when low energy electrons are expected to be absent, the averages of $f_\perp$ and $f_\parallel$ are both near their instrumental background level and their ratio is greater than 1.1 only 13% of the time. During away sectors where polar rain electrons are expected to be present, the ratio is greater than 1.1 90% of the time. The absolute average intensity for $f_\parallel$ was 1.65×10^{-29} s^3 cm^{-6} for away sectors at 180 eV, a value 2.4 times higher than for toward sectors. This factor undoubtedly would have been higher except for the fact that low values in toward sectors were limited by the instrumental threshold.

Figure 4 is clearly in agreement with the previously reported polar rain dependence on interplanetary sector structure and we conclude that the anisotropic lobe electrons are indeed the magnetotail component of the polar rain. We proceed to investigate the relationship of these electrons to the solar wind.

4. Interplanetary Origin of the Polar Rain

Although access of solar wind electrons has been suggested as the source for the polar rain, little consideration has been given to whether asymmetries in the observed solar wind distribution functions are quantitatively compatible with the north-south polar cap asymmetry. Now, the additional observation that the magnetotail source of polar rain electrons is highly anisotropic puts a new, stringent constraint on the solar wind origin hypothesis. Rather than simply requiring that the average solar wind flux be consistent with magnetosphere observations [Fennell et al., [1975], or more specifically that the field aligned solar wind electrons are consistent, we must now ask whether complete solar wind distribution functions, when mapped

along field lines into the higher fields of the magnetotail, are consistent with the observed anisotropy. As will be illustrated below, such compatibility is far from evident since theory indicates that the particle distributions tend to become more isotropic when mapped to a stronger field region.

4.1 Mapping Interplanetary f

The solar wind distribution function f can be represented as the sum of three maxwellian or bi-maxwellian components.

$$f=f_c+f_h+f_s \qquad (1)$$

The "core", f_c, and "halo", f_h, are well known components of the solar wind [Montgomery et al.,1968]. The core, is a cool component with temperature $\simeq 1\times10^5$°K which accounts for about 94% of the solar wind density [Feldman et al., 1975]. This cool component is important only at very low energies ($\lesssim$40 eV) that are either below our measurement range or in channels contaminated by the spacecraft plasma sheath; we ignore this component in the present discussion. The "halo" component, f_h, can be approximated as a maxwellian with higher temperature and lower density,

$$f_h = n_h/(\pi^{3/2}\omega^3)\exp(-v_\parallel^2 - v_\perp^2)/\omega^2 \qquad (2)$$

where $\omega^2 = 2kT_h/m_e$ and $T_h \simeq 8\times10^5$.

The "strahl", f_s, is a field aligned component which was not discovered until measurements from relatively narrow angle detectors on the Helios spacecraft were surveyed [Rosenbauer et al., 1976; 1977]. Earlier surveys had used detectors with apertures that were large compared with these field aligned electrons and hence the intense directed fluxes were indistinguishable from weaker broadly distributed fluxes. The strahl has subsequently been confirmed by Feldman et al. [1978] and Ogilvie and Scudder [1981]. It is thought to be due to electrons of the solar corona which reach the vicinity of

1 AU with few collisions and minimal scattering [Rosenbauer et al., 1976; 1977; Olbert, 1981] (see section 6). These electrons are very field aligned because they tend to conserve their first adiabatic invariant ($\mu \propto v_\perp^2/B$) as they move away from the sun in the decreasing solar (interplanetary) field. The lower energy strahl electrons are scattered more than those at higher energies due to the strongly energy dependent coulomb collision frequency, and therefore lower energy strahl electrons are observed to be more isotropic than those at higher energies [Rosenbauer et al., 1976; Olbert, 1981; 1983]. The halo distribution may in fact be simply the lower energy corona electrons that have been scattered enough to make them fairly isotropic [Rosenbauer et al., 1976; Scudder and Olbert, 1979a,b]. A more detailed discussion of the escape of strahl electrons from the sun will be given in section 6. For the present we note that these electrons are important in carrying the interplanetary heat flux and they have a preferred direction of motion away from the sun and along the local magnetic field. This motion gives them the potential for preferentially entering one polar cap or the other and thus explaining the north-south asymmetry of the polar rain. We model this anti-sunward moving strahl as a third bi-maxwellian

$$f_s = n_s/(\pi^{3/2}\, \omega_{s_\parallel}\, \omega_{s_\perp}^2)\, \exp(-v_\parallel^2/\omega_{s_\parallel}^2 - v_\perp^2/\omega_{s_\perp}^2) \qquad (v_\parallel>0) \qquad (3)$$

where $\omega_{s_\parallel}$ is considerably greater than $\omega_{s_\perp}$.

To map an initial distribution function at point 1 (e.g. the solar wind) along a field line to point 2 (e.g. the tail lobe), we assume conservation of energy

$$(1/2)mv_{1_\parallel}^2 + (1/2)mv_{1_\perp}^2 - e\phi_1 = (1/2)mv_{2_\parallel}^2 + (1/2)mv_{2_\perp}^2 - e\phi_2 \qquad (4)$$

and conservation of the first adiabatic invariant

$$\mu_m v_{1_\perp}^2 / B_1 = v_{2_\perp}^2 / B_2. \tag{5}$$

Combining these equations we can express the initial velocities at point 1 in terms of the final velocities at point 2 as

$$\begin{aligned} v_{1_\perp}^2 &= (B_1/B_2) v_{2_\perp}^2 \\ v_{1_\parallel}^2 &= v_{2_\parallel}^2 + (1-B_1/B_2) v_{2_\perp}^2 - 2e/m\ (\phi_2 - \phi_1) \end{aligned} \tag{6}$$

Invoking Liouville's theorem and assuming the field varies monotonically between points 1 and 2 to assure particle access to the stronger field, we know that f is conserved along the particle trajectory. Taking a velocity at point 2, we can find the equivalent velocity at point 1 from (6), evaluate f at point 1 from (1) and know from Liouville's theorem that it is the appropriate f for point 2.

We have carried out this procedure and contours of f in the $v_\parallel$, $v_\perp$ plane are shown by the lighter curves in Figure 5. Figure 5a contours are calculated directly from equation 1 (neglecting f_c) while those of 5b represent the distribution mapped to a field which is 2.7 times the interplanetary field strength. We have assumed that $\phi_2 - \phi_1 = 0$ here and in subsequent discussions. In equation 1 a solar wind halo temperature and density of 5×10^5°K and .1/cc was assumed along with a strahl temperature $T_{\parallel_S} = 1.5 \times 10^6$, $T_{\perp_S} = 2.6 \times 10^5$ and $n_S = .086$. These parameters were chosen to represent the data in Figure 2 and their selection will be discussed below. The contours in Figure 5a are elongated along the $v_\parallel$ axis and are very similar to the strahl examples shown by Rosenbauer et al. [1976; 1977], Feldman et al., [1978] and Ogilvie and Scudder [1981] but are quite different from the

more isotropic solar wind contours deduced from earlier wide angle solar wind instruments [e.g. Feldman et al., 1975] which were widely known at the time of the Mizera and Fennell review [1978].

As the solar wind electrons move into the stronger field, conservation of μ requires that their perpendicular speed increases in proportion to $\sqrt{B}$ until all their energy is in $v_\perp$, at which point they mirror and return to the solar wind. Only electrons from the shaded region in Figure 5a (those with pitch angles less than 37.5°) reach field strengths of 2.7 B_1 (Figure 5b) where they fill the entire $v_\parallel, v_\perp$ plane. The contours in Figure 5b are noticeably less anisotropic even for this modest field increase. Those electrons that reach low polar cap altitudes experience a field increase of roughly 5000. They will be even more isotropic than in Figure 5b because they all come from a solid angle in the solar wind of less than 1°. There is not apt to be a very large anisotropy within such a small solid angle and hence the low altitude distributions are expected to be much more isotropic. Note that the contours intersect the $v_\parallel$ axis at identical points in 5a and 5b indicating that the electrons moving precisely along the field ($v_\perp$=0) are unaffected by the changing field.

Since most of the electrons passing a given point in the tail lobe will mirror at lower altitudes and move back out of the tail (excepting those within the very small and essentially unmeasureable loss cone of less than a few degrees) the fluxes should show little parallel-anti-parallel asymmetry relative to the field direction. This is what is observed by ISEE 1 in the tail lobes (e.g. Figure 2).

Constant energy circles are overlayed on the distribution function contours of Figure 5a and 5b at the measured ISEE energies of 87 and 510 eV. Measurements made at various pitch angles along these constant energy circles

will show a decreasing f as the sampled pitch angle becomes closer to 90°. Plots of log f versus pitch angle from the mapped model distribution are superimposed on the data of Figure 2 as smooth curves. Clearly both the absolute magnitudes and the pitch angle dependence of the model fit the data quite well. At high energies the model anisotropy is maximal due to the anisotropic strahl while at lower energies the distribution is more isotropic due to the increasing influence of the lower temperature, more nearly isotropic halo. This lower anisotropy at lower energies is a very common feature in the tail lobes as it is in the solar wind [Rosenbauer et al., 1976] and it thus supports the idea that the solar wind is the source of the polar rain.

The technique used for determining the solar wind halo and strahl density and temperatures from tail-lobe data is illustrated with an example shown in Figure 6 and 7. The lower portion of the Figure 6 shows the log f versus pitch angle plots on March 10, 1978 in the format of Figure 2. At this time the experiment was in the higher energy mode extending to 7 keV but all energies above 1 keV were measuring background levels and those above 1.35 keV are not shown. At the top of Figure 6 we show plots of f versus $v_{\parallel}$ and $v_{\perp}$ which are the orthogonal cuts through a three dimensional surface fit to the measurements [Fitzenreiter et al., 1984]. Using such fitted data is a slight improvement over the measured points since the measurements are made at pitch angles close to but not exactly at zero. In Figure 7 we plot the log of these fitted f values versus $v_{\parallel}^2$. On this type of plot a maxwellian distribution appears as a straight line. At the highest energies we assume that only the strahl is important; we then can obtain the strahl parallel temperature (2×10^6°K) from the slope of this line and the coefficient of the strahl exponential from the intercept with the ordinate. For a maxwellian with a

single temperature this intercept would define n_s, but with a two temperature bi-maxwellian it only defines a relation between n_s and $T_{s\perp}$ and further information from other pitch angles must be utilized to specify n_s or $T_{s\perp}$. In this case we find $n_s = .012$ and $T_{s\perp} = 1.3 \times 10^5$°K. In principle the same technique can be used at lower energies where the halo dominates, but sometimes, as in Figure 7, there are not enough energy channels to define this slope. However, the pitch angle dependence of the data together with the limited energy interval may be combined to determine appropriate halo parameters ($T_{h\parallel} = 5.5 \times 10^5$°K, $T_{h\perp} = 1.5 \times 10^5$°, and $n_h = .1/cc$). A low energy slope determined in this way is shown on Figure 7. Winningham and Heikkila's [1974] polar rain spectrum is superimposed for comparison and it shows a very similar temperature. The values from the model distribution mapped to the tail are also superimposed on Figure 6a and the very good agreement is apparent. These temperatures only characterize the more field aligned portion of the interplanetary distribution (equivalent to the shaded portion in Figure 5a) and hence may not give a value of $T_\perp$ equivalent to that determined from the entire interplanetary distribution. The $T_\parallel$ halo values are, however, typical of the solar wind [Feldman et al., 1975]. This agreement between model parameters determined in the tail and typical solar wind parameters strongly supports the concept of solar wind entry.

About four hours before the data in Figure 6a was taken, ISEE had observed the tail lobe at lower altitudes where the field strength was about 100 nT or twice the value in 5a. This data is shown in Figure 6b. The curves from the model are again superimposed using the same solar wind parameters determined from 6a, correcting only for the greater lobe magnetic field

strength. The good agreement can be attributed to the validity of the mapping procedure and the stability of the source conditions over the intervening time. In neither case were field aligned potentials invoked.

We note that the strahl temperatures determined in the above manner are typically 2×10^6°K. This corresponds very well to the canonical value of the solar corona as would be suggested by an exospheric treatment [Schulz and Eviatar, 1972] and thus tends to further substantiate our proposed origin of these electrons observed in the tail lobes. We discuss this point more fully in section 6.

5. Energetic Polar Cap Electrons

One of the most interesting aspects of polar cap electrons are the less frequent occurrences of spatially uniform, higher intensity precipitation seen at energies up to about 10 keV. As was mentioned above, this phenomena has generally been considered as a separate class of event which requires a field aligned magnetospheric acceleration mechanism. However, in view of our proposed association between the solar wind strahl and the polar rain, it is of interest to reexamine this problem and ask whether the characteristic variations in the strahl which have been reported [Rosenbauer et al. 1976; 1977; Feldman et al., 1978; Pilipp et al., 1981; Pilipp, private communication, 1984] might explain these low altitude observations and eliminate the need for magnetospheric acceleration.

Existing information on high intensity polar cap electrons has come from 4 events of roughly a day or two duration centered on December 20, 1971, March 10, 1972 [Foster and Burrows, 1976], September 18 1974, and October 15 1974 [Meng and Kroehl, 1977]. All four events show intense precipitation preferentially on the northern polar cap and all events for which

interplanetary data is available (the latter three), are associated with away sectors. Also all the events are associated with magnetic storms; Foster and Burrows [1976] note that their events are associated with post storm quieting and to some extent the same appears to be true with the events of Meng and Kroehl [1977].

Available solar wind data for these events is presented in Figure 8. Solar wind speed, density and proton temperature [King, 1979; 1983] are plotted versus time and shading indicates the approximate time and duration of the polar cap events. The March 10, 1972 event (Figure 8a) occurs as the speed decreases a few days after the arrival of a high speed stream on March 6 which was probably caused by a transient event on the sun. The polar cap event is closely associated with unusually low density solar wind of less than 1/cc which caused the earth's bow shock to move out beyond the IMP-6 spacecraft which was located more than 25 R_e upstream of the earth [Fairfield and Feldman, 1975]. The September 1974 event of Meng and Kroehl (1977) is characterized by large polar cap ratios on September 16 which then decreased before increasing to even higher values on September 18. These two intervals are identified separately in Figure 8b. The first interval closely follows the arrival of a corotating solar stream and the second more intense event is associated with the latter stages of a very low density region as was the case on March 10, 1972. The October 15 event (Figure 8c) occurs one solar rotation later and is associated with a corotating stream. The density averages 6/cc during this interval.

ISEE 1 spent only 89 hours (Figure 4) in the tail lobe in 1978 when conditions were appropriate for the solar wind strahl entry to the northern hemisphere. Consequently it is not surprising that ISEE did not see any polar rain events as intense as those selected from the larger DMSP and ISIS data

sets. The example shown in Figures 6 and 7 is in fact a relatively intense event for ISEE and meaningful counting rates were seen as high as 761 eV. The interplanetary density was below 4/cc during most of this day.

For these few examples then, it appears that the solar wind tends to have unusually low densities at times of more intense polar rain. Note that this observation is contrary to what one might naively expect - that increased solar wind density would produce increased polar cap precipitation. We will return to this point after reviewing ideas on the strahl formation in the next section.

Other important information about intense polar rain can be deduced from the shape of the distribution function. We have scaled points from Figure 3 of Foster and Burrows [1976] and Figures 5 and 7 of Meng and Kroehl [1977] and these points, converted to distribution function f, are plotted versus energy in Figure 9a. Again quasi-maxwellian regimes will appear as straight lines. For reference we reproduce the two fitted distributions from our relatively intense ISEE example of Figure 6-7 where counting rates fall below the instrumental background above 1 keV. The shape of the distribution functions for intense polar rain events shows a general resemblance to the ISEE data that is characteristic of more normal polar rain. The Foster and Burrows data, which extend to low energies, have a low temperature component which is more intense than normal polar rain but has a "temperature"

$$d\log f/dE = -1/k"T" \qquad (7)$$

similar to low energy ISEE polar rain and the solar wind halo. Between 200 eV and 700 eV all the intense events have high intensities but they have strahl-like "temperatures" of roughly 2×10^6°K which are comparable to the ISEE data. The additional feature revealed by the intense events is a high energy tail above approximately 1-2 keV. We note that the intense polar rain spectra

are consistent with being proportional to the more typical ISEE polar rain, if we assume that the high energy tails for the intense events are due to intensity changes which raise the >2 keV tail above particle detector threshold. In the next section we review current ideas on the escape of electrons from the sun before concluding that intense polar rain data are compatible with a solar origin hypothesis.

6. Electron Escape from the Sun

The current theoretical understanding of the formation of the solar wind strahl suggests that it is shaped en route from the sun by the competition between two forces. On the one hand coulomb scattering broadens the distribution while on the other hand the Lorentz force, which in the absence of collisions is normally discussed via conservation of the first adiabatic invarient μ, tends to induce a field aligned collimation [cf Jockers, 1970]. The parameters that determine the importance of these forces are the flux tube profiles of density, temperature, and magnetic field strength. The coulomb scattering frequency $\nu_s \sim \nu_o (n/n_o)(T_o/T)^{3/2}(E_o/E)^{3/2}$ is strongly energy dependent whereas μ conservation implies that the logarithmic rate of change of pitch angle is essentially independent of energy. Together these facts imply that there is significant energy dependence in the relative importance of the forces that shape f near 0° pitch angle. At sufficiently high energies the magnetic focusing makes f very nearly field aligned because coulomb collisions cannot broaden it. At low solar wind "core" energies the coulomb collisions dominate [Scudder and Olbert, 1979a] and the distributions are nearly isotropic. At intermediate energies there is a gradual transition and closer competition among the two effects.

The approximately field aligned ($v_{\parallel} > 0$) "strahl" regime of the halo is most easily thought of as the least coulomb screened remnant of the inner coronal regions as illustrated by Scudder and Olbert [1979a, eqtn 11] where (in the high energy limit)

$$f_{\bullet}(E_{\bullet}, \mu=0) = f_{o}(E_{o}, \mu) \exp(-S(E_{\bullet}, E_{o}, n, T)) + \text{low energy correction} \quad (8)$$

Here $f_{\bullet}$ is the distribution function at earth, while f_{o} is the corresponding quantity in a region of rapidly decreasing density at 1.03 R_{o}. The appropriate form of f_{o} is not known a priori, but it surely depends on the density and scale heights in this vicinity. At times when coronal densities attain higher or lower values, the function f_{o} will in general change. In equation 8, S is an energy and path dependent counter of the number of collisions a fictitious "collisionless" particle would have encountered getting to the observer: $S = \int \nu(E(t),t)dt$, where ν is the collision frequency at time t along the particle trajectory. Note that the energy E(t) of the electrons leaving coronal altitudes is reduced by climbing up the heliospheric potential barrier. This raises the local collision frequency and makes S a spatial integral over the local collisional frequency and the potential between the sun and earth. The coulomb terms become increasingly important as the local kinetic energy is reduced and or as the effective path length is increased due to the pitch angle increasing.

The energy dependent counter S determines the opacity of the coronal distribution function f_{o} to the local observer. This opacity is determined by the radial profiles of the electron density, temperature, and heliospheric potential. In the high energy regime, where (8) is approximately valid, S' affects f in a simple way given by

$$\log_{10} f_{\bullet} \cong \log_{10} f_{o} - S'(n,E) + \ln(\text{correction}), \quad (9)$$

where $S' = S \times \log_{10} e$, is the energy dependent number of decades f_{o} is reduced

to produce $f_\bullet$. Figure 9b illustrates $S'(n,E_\bullet)$ which has been calculated for two different coronal density profiles corresponding to a polar coronal hole [Munro and Jackson, 1977] and an equatorial region. (Parameters for these profiles are from Olbert [private communication, 1978] and correspond to 1 AU densities of 4.8/cc and 15.4/cc. The electron temperature has been assumed to vary as $n^{1/6}$ which implies that the heliospheric potential energy drop between point r and infinity is 7kT(r) which distills the results of Sittler and Scudder [1980].) The quantity S' is large at energies below the heliospheric potential energy ($\stackrel{<}{=}$750 eV) where scattering dominates but as E increases, S' rapidly becomes very small for both profiles. Although S' never attains a value of zero indicating a complete absence of screening, we adopt a value of S' = 0.5 as an effective lower bound on a high energy region where screening is not important. Above this energy, E_ν^*, the spectral shape at 1 AU is little modified from f_o. Figure 9b shows that E_ν^* is higher for the higher density profile. Because of the exponential screening factor this leads to the important expectation that higher (lower) column densities should strongly depress (enhance) strahl phase densities.

The portion of f_o that reaches 1 AU is shown explicitly in Figure 9c. Here we have taken the Foster and Burrows polar cap spectrum from Figure 9a which was obtained at a time of very low solar wind density. The top curve is spline approximation to the essential features of this spectrum. The heavily shaded region plus the diagonally shaded region of this figure represents that portion of f_o calculated as surviving at 1 AU if the heavy curve were assumed to be the actual coronal boundary condition and realistic low density conditions prevail. Above 200 eV the observed and primary spectrum are nearly identical and in the usual polar rain regime 200-500 eV range the slope is essentially that of f_o in the corona. The diagonally shaded region indicates

what would remain from the same solar spectrum if the column density were high. This diagonally shaded region is strongly depressed relative to the low density case indicating that the observed distribution in the usual polar rain regime has a slope that is severely modified. In fact the actual slope in this region (not shown) will be that of the nearby (cooler) halo which will fill in the low energy void (i.e., the low energy terms neglected in equation 8). Notice that the slopes of the data curves (Figure 9a) in the 200-500 eV range are most nearly coronal ($2x10^6$) for the low density and or high speed examples in Figure 9a and cooler for higher densities.

The above theoretical concepts are in agreement with much of what is known about the strahl. Experiments (generally at E<1 keV) have shown that the strahl is most prominent (intense and narrow) in high speed streams [Rosenbauer et al., 1976; Pilipp et al., 1981] where the density is on average low Feldman et al., 1978]. At 1 AU the solar wind number flux, nV, tends to be constant on average (Bridge, 1976), although this relation need not strictly hold in individual cases. In comparisons with the data that follow, we will use the locally measured density as the observable most closely related to the integrated column density. At the same time we will remember that local density enhancements may occur and that high speeds may be an additional indicator of low column densities.

Little is known about the strahl in the solar wind above 10 keV since its narrowness makes it is very difficult to detect. Strahl "temperatures" (in the sense of equation 7) at solar wind electrostatic analyzer energies ($E \simeq 300$ eV) have been reported between $7x10^5$ [Ogilvie and Scudder, 1981] and $8.9x10^5$ [Feldman et al., 1978] and as high as $2x10^6$ [Rosenbauer et al., 1976]. The

latter authors noted that no single maxwellian characterized the entire energy range in the strahl direction with the highest T estimates (in the sense of 7) associated with the highest halo energies ($\lesssim$1keV).

The labels of the intense polar rain spectra in Figure 9a have been arranged in order of increasing 1 AU solar wind densities. At one extreme in Figure 9a the two most intense polar rain spectra in the 200-500 eV range correspond to an unusually low solar wind densities of 0.6 and 0.9/cc. The fact that no solar wind antecedent could be found for the Foster and Burrows particles by wide aperture solar wind electron detectors is consistent with the theoretical prediction that maximum field collimation (producing maximum difficulty of detection) would be expected at this time. At the other extreme, the Fennell et al. example which revealed similar polar cap and solar wind intensities occurred when the solar wind density was upwards of 20/cc. Under these conditions the field aligned component is theoretically expected to be significantly depressed and broadened. The other high intensity cases abstracted from those of Meng and Kroehl either occur at similarly low densities or accompany relatively high speed solar wind >550 km/s. Together these examples reveal an association of high intensity polar rain and extremely low density and or high speed solar wind at 1 AU.

Although column density variations can explain the strahl intensity changes at intermediate energies (E $\lesssim$200-500 eV) where electrons are scattered away from field alignment to a greater or lesser degree, at higher energies field alignment always prevails and hence the variations of S' cannot explain the higher energy intensity changes. At these higher energies (where S' <0.5) the 1 AU observer sees an essentially unscreened f_o; the question thus becomes how does f_o vary near 1.03 R at these times. Since high intensities appear to be associated with low densities and high speed streams we consider solar

conditions at these times. These wind conditions are widely held to result from extremely low density and or rapidly diverging magnetic topologies over coronal holes [Holzer, 1977; Levine et al, 1977]. These regions also have stronger density gradients than regions where slower flows appear to originate [Munro and Jackson, 1977].

It is indeed reasonable that f_o depends on the absolute coronal densities and scale heights at 1.03 R_o. In particular, in the presence of strong gradients in a fully ionized plasma at the surface of a star it is very difficult to guarantee a priori that a Maxwell Boltzman distribution would adequately describe the highest local kinetic energies. In fact it is very difficult to surpress the non-thermal tails [Scudder and Olbert 1979a, b, 1983], especially in the steep coronal hole density profiles which also have low absolute density. These tails usually appear at approximately 7 times the local most probable energy particle [Scudder and Olbert, 1979,a b] which at coronal temperature of kT $\simeq$170-200 eV implies significant, flatter non-thermal tails above break energies of 1190-1400 eV at the sun. At the orbit of earth these electrons have given up kinetic energy to the heliospheric potential (500 to 1000 eV). Modest net energy shifts are anticipated across the bow shock-magnetopause so estimates of net energy shifts for the breaks in the injection spectrum at earth are between 425 and 1000 eV. This regime is compatible with Figure 9a which shows a transition from $(-kT)^{-1}=d\ln f/dE \simeq 1.5-2\times10^{6}$°K in the regime 200-300 eV with transitions to flatter tails occurring at energy from $\simeq$500 eV for Foster and Burrows to 1300 eV for Meng and Kroehl.

An exciting aspect of polar solar measurements is that the magnetic defocusing of the strahl over a collisionless traversal of the shock, sheath and and lobe, allows a much better view of f_{theory} along B because it takes the narrow bundle of phase space and disperses it over a much wider solid

angle so that f_{obs} ($\langle v_\perp \rangle = 0$) in the magnetotail or even better at lower altitudes is essentially f_{theory} ($v_\perp = 0$), a quantity most directly related by exospheric theory to the coronal boundary conditions f_o [Schulz and Eviatar 1972]. Recall that in these exospheric theories, there is no guarantee that the boundary condition of f_o equal to a Maxwellian is physically warranted. Polar cap measurements of the high energy form of $f_\bullet$ can help establish f_o and contribute to the longstanding issue of how to energetically support the high speed solar wind state seen at 1 AU.

The detection of the supra-coronal thermal spectrum has profound implications for indirectly determining the coronal temperatures from the interpretation of optical emissions from the coronal regions and the freezing in of coronal charge states sampled in the solar wind [Owocki and Scudder, 1983; Owocki, 1982]. The existence of strongly suprathermal distributions at the base of the solar wind expansion has also been previously suggested by Scudder and Olbert [1983] and Olbert [1982;1983] as being required for a conduction supported high speed solar wind. Finally it is of interest to estimate the implications of the polar cap observations of f to determine the implied temperature of the coronal electrons (in the sense of P/nk) and contrast it with the upper bounds of $T = 2 \times 10^{6\circ}K$ suggested by Leer and Holzer [1979]. Assume a two maxwellian approximation for $f_\bullet$ above E=100 eV. Let T_{co} be the effective "temperature" for 100 eV< $E_\bullet$ <400 eV and T_{ho} the corresponding quantity for the flat tail regime. Let their corresponding densities be n_c° and n_h°. Let the potential energy difference to $r = 1.03\ R^\circ$ be given by $e\Delta\phi$. Using the values fit to Foster and Burrows in Figure 9 yields $n_h/n_c \lesssim 0.05$; $T_h^\circ \lesssim 10 T_c^\circ$; assuming $e\Delta\phi = 750$ eV implies that $T_o \lesssim 1.009\ T_{co}$ or that monitoring T_{co} we essentially monitor T_o. Thus the presence of the suprathermal tails, a few percent by number in the corona with a high

"temperature", does not contradict the coronal bounds of and are consistent with arguments of Leer and Holzer [1979].

7. Summary and Discussion

In this paper we have presented new evidence that polar rain electrons observed in the magnetotail are highly anisotropic in the field aligned sense. We have used this stringent new observational constraint to test the solar wind entry hypothesis. We find support for this idea based on the quantitative agreement between lobe measurements and typical solar wind distribution functions mapped to the tail lobes. Furthermore we find that it is the solar wind strahl portion of the suprathermal electrons which is responsible for both the tail lobe anisotropy and electron precipitation over a preferred polar cap. Alternative explanations fail to provide such agreement; the more traditional and more isotropic core and halo solar wind electron distributions known at the time of Fennell et al. [1975] would become even more isotropic when they enter the tail and hence they fail to explain the observed lobe anisotropies.

Although acceleration by a field aligned electric field might seem like a method for introducing such an anisotropy, this does not appear to be a valid alternative. A field aligned electric field along an intensifying magnetic field does not preferentially accelerate field aligned particles within a hot population. Although field aligned particles are accelerated, those with slightly larger pitch angle are also accelerated and isotropy tends to be preserved. Only if one accelerated a very cold distribution with low $v_\perp$ spread can one preferentially produce field aligned electrons and avoid the accompanying less field aligned electrons as B increases and $v_\perp^2/B$ is

conserved. If the solar wind core electrons were accelerated to give the observed anisotropy, the phase space density and temperatures would not match the tail observations.

7.1 Magnetospheric entry

We summarize our views of electron entry to the magnetosphere using Figure 10 which schematically illustrates electron distribution function contours relative to the magnetic field in various spatial regions. All distributions are supported by solar wind and magnetosphere measurements described above or magnetosheath measurements discussed below.

Distribution 1 in undisturbed interplanetary space is the halo-strahl distribution with the asymmetry provided by the almost collisionless strahl electrons streaming out from the sun. Note that the halo-strahl distinction is a convenience for modeling and describing a distribution function that gradually changes from highly anisotropic to isotropic with decreasing energy; in reality the low energy isotropy is probably due to the highly-scattered, outward-moving coronal electrons that would be highly anisotropic in the absence of collisions. The shaded area along the field direction schematically illustrates those electrons destined to precipitate on the polar cap if the field line connects to the tail. In distribution 1 the actual angular width of the region is of the order of 1°. Distribution 2 is the field aligned population measured by ISEE 1 on tail lobe field lines that connect to field lines leading back to the sun. The distribution is field aligned due to strahl electrons freely entering the tail but it is less anisotropic than in the solar wind due to the effect of the electrons moving into the stronger lobe field. The distribution is bi-directional because most of the electrons passing ISEE mirror at lower altitudes and return to the spacecraft to produce the nearly symmetric distribution. Only the most field

aligned electrons within about 2° of $\hat{B}$ precipitate and produce the polar rain. The upcoming loss cone should be devoid of solar wind electrons because these particles have precipitated. This region may be populated by ionospheric sources, but it is too narrow to be measured by ISEE. At low altitudes over the polar cap the distribution is much more symmetric and the loss cone fills most of the down coming hemisphere (distribution 3).

In the other tail lobe where the reconnected field lines lead to interplanetary lines that do not lead directly back to the sun, only the more isotropic sunward half of the interplanetary distribution (the halo) enters the tail. This distribution mirrors and produces distribution 4 which is isotropic except for the empty loss cone. ISEE only measures these isotropic electrons at low energies in the "unpreferred" polar cap. The quasi-isotropic halo is seen over both polar caps but over the preferred cap it is supplemented by the anisotropic electrons of the strahl. The presence of the energetic strahl electrons over one pole but not the other leads to large north-south asymmetries at high energies. The more isotropic low energy distributions over both polar caps leads to decreasing north-south asymmetries at these lower energies. Changing solar-interplanetary conditions will raise or lower the energy where the north-south asymmetries become large.

In the magnetosheath an anisotropic distribution 5 would be expected on field lines that simply continue on downstream of the earth. This distribution would be reversably broadened but its field aligned asymmetry preserved. Where solar particles traverse the thinnest perpendicular portion of the subsolar bow shock they remain magnetized for gyroradii $r_e << 15$ km which is the thinnest scale of the perpendicular shock [Scudder et al.1984]. This implies that electrons with energy below $\sim$500 eV only gain energy from the deHoffman-Teller frame electrical potential which is $\stackrel{<}{\sim}$30-80 V [cf Goodrich and

Scudder, 1984]. Higher energy electrons with larger gyroradii could gain energy of up to 200-300 eV across a perpendicular shock, but less across a quasi-parallel shock. In reality, most polar rain electrons will approach the more distant magnetopause having traversed a weaker distant bow shock where they will have gained much less energy than the worst case numbers above. Distribution 6 or 7 ought to be seen on magnetosheath field lines that connect to the tail. Which of these distributions is seen will depend on which polar cap the distribution is mirroring in.

The anti-sunward moving half of the anisotropic magnetosheath distribution (5 or 6) has probably been seen by the Apollo plasma detectors on the surface of the moon [Reiff and Reasoner, 1975]. They frequently detected two maxwellian components in the magnetosheath with the hotter component having temperatures and densities of 2.5×10^6 and .05/cc which are similar to the then unknown strahl. This component was anisotropic (different intensities in two detectors looking in different directions) and time variable. Although these authors suggested bow shock electron acceleration as the cause, in retrospect it seems quite possible that a varying magnetic field was moving the anisotropic strahl in and out of the fields of view of their detectors.

Since we advocate the entry of solar wind electrons to the tail lobe, it might be thought that the low energy, high density electrons should also enter the magnetotail. Such entry would be contrary to longstanding evidence for low density lobes, an observation confirmed indirectly on ISEE by the existence of a spacecraft plasma sheath that would not occur in the presence of a higher density plasma. We suggest that the lack of intense low energy electrons involves the behavior of protons. The low energy electrons, having much higher speeds and greater mobility than protons, could easily follow the

field lines into the magnetosphere, but to do so would produce field aligned currents and an unacceptable charge imbalance. We propose that a field aligned thermal potential is created near the tail magnetopause to prevent such low energy electron entry. This potential drop will occur across the strong density gradient in the reconnected flux tube discussed by Sibeck and Siscoe, [1984]. This potential will adjust itself to allow the appropriate number of electrons to enter consistent with the rotational discontinuity mass flux requirements.

We emphasize that this magnetopause potential decelerates the entering electrons whereas previous work (e.g., Foster and Burrows, 1977; Gussenhoven et al., 1984) has concentrated on accelerating tail lobe electrons. In our picture the bow shock accelerates the electrons while the magnetopause decelerates them to a somewhat greater extent. This situation leads to tail lobe energies slightly reduced relative to the solar wind that are still consistent with our earlier assumption of $\phi=0$ made while comparing ISEE measurements with typical solar wind strahls.

Furthermore we suggest that the magnitude of this magnetopause potential will be related to the location where the field line enters the magnetopause. On magnetospheric cusp field lines the potential as a fraction of the magnetosheath electron temperature will be small and large fluxes of hot, magnetosheath electrons and their accompanying protons will enter as is observed [e.g., Winningham, 1972]. On field lines poleward of the cusp the ions cool faster than the electrons, and simultaneously the magnetosheath density is reduced as the flow increases. Both these changes imply that increased decelerating potentials are required to permit ever smaller fluxes of electrons (and ions) to move down lobe field lines. A calculation of this potential profile demonstrates that the equilibrium electron flux (mean

energy) is most intense (lowest) near noon and is more than one order of magnitude larger (factor of 3 lower) than the fluxes (mean energy) near midnight. This noon-to-midnight variation in intensity is anti-correlated with energy and is the main experimental finding in the recent paper of Gussenhoven et al. [1984]. These authors suggested that internal magnetospheric processes were the probable cause of this morphology. Our suggestion is that the polar rain electrons come directly from the coronal solar wind with magnetopause boundary condition systematics modulating their mean intensity and energy. Energization need not occur anywhere within the magnetosphere.

7.2 Solar Source

Once the strahl was established as the source of polar rain electrons, we asked the further question of how the strahl is produced by the sun. Current thinking is that the strahl is due to the nearly collisionless escape of electrons from the corona, with the collimation along the field direction produced by adiabatic focusing in the decreasing solar-interplanetary magnetic field. An energy dependent collision frequency dictates that different energies will arrive at 1 AU with different anisotropies.

Lower energy electrons should undergo frequent collisions and be severely scattered. In this manner the quasi-isotropic halo will be produced from electrons that would otherwise have been field aligned. At slightly higher energies there ought to be a closer competition between scattering and the tendency toward field alignment. Lower solar wind column densities will tend to make field alignment prevail and produce higher field aligned intensities that extend to lower energies. Effective "temperatures" in this intermediate energy range should correspond to coronal values. For higher solar wind

densities, scattering will prevail, reducing field aligned intensities, and shaping a more isotropic, cooler, halo-like distribution.

At still higher energies, electrons with lower collision frequencies should make the transit to 1 AU with little scattering regardless of column density. They will become very field aligned at 1 AU and preserve the true characteristics of the high energy spectrum at the solar source. At these higher energies we must look to variations at the solar source to produce variations at 1 AU. We noted that times when the low column densities will produce enhanced strahl formation tend to be associated with high speed streams and low densities. These conditions are thought to originate from the central regions of coronal holes where the density is low and the scale heights of density and magnetic field are shorter than in the source regions for the slow, dense solar wind. It is, therefore, more difficult to suppress suprathermal tail formation in these regions than elsewhere. Accordingly, it is expected that f_o above source regions for fast, sparse solar wind flows should be preferentially more non thermal and intensities at higher energies should be enhanced. This implies that an observer at 1 AU who is essentially unscreened from the corona at sufficiently low energies may see signatures of the statistical equilibrium in the corona, including the production of a non-thermal distribution with a "temperature" which is nearly 2×10^6°K.

7.3 Energetic Polar Cap Precipitation

The above concepts are in fact supported by observations. First of all an enhanced strahl is associated with high speed streams which in turn are known to be associated with low densities. We also noted the similarity of the f versus E plots in Figure 9a for the intense events and the more normal polar rain. Of particular note was the common $\simeq 2 \times 10^6$°K coronal-like "temperature" (i.e. slope) in the energy range $\simeq$200-700 eV. In fact the

primary difference between the normal and intense events seems to be proportionately higher fluxes and the presence of a high energy tail above about 1 keV during the intense events. This high energy tail could well be present during the more normal events, but at these lower intensity levels it would be below instrumental background. Finally we noted that the intense events seem to be associated with intervals of an usually low solar wind density which, as was pointed out above, is the 1 AU condition for pronounced strahls.

Arguments against a solar origin given by Foster and Burrows [1976] were (1) the non detection of high fluxes of interplanetary source electrons at the time of intense polar cap precipitation events, and (2) the similarity of the spectrum of polar cap and plasma sheet electrons which they felt implied a common source. With modern information on the observed narrowness of the strahl and the expectation that still higher energy electrons would be even more collisionless and field aligned, it now seems quite likely these electrons would have eluded detection by the wide angle detectors available at that time. As for point 2, we agree that the two spectra are similar, but the solar wind/corona could equally well be the common source for these two regions on March 10 1972; the electrons could have E x B drifted onto closed plasma sheet field lines or they could have become trapped on field lines that became closed due to tail reconnection.

7.4 Conclusions

Based on the quantitative mapping of modern solar wind measurements to the tail lobe we conclude that normal polar rain is of solar origin. We explain existing measurements with a solar wind entry model that does not require accelerating field aligned potentials. A more rigorous solution to the complete polar electrodynmics problem that considered atmospheric

photoelectrons and polar wind populations might well require weak field aligned potentials, but their effect on the polar rain at energies $\gtrsim$100 eV is probably minimal. Unusually intense polar rain seems to appear at times when the strahl is expected to be especially prominent and solar electrons are apt to be intense. Hence direct solar access seems to provide a simple, viable explanation for intense polar rain as an extreme of coronal boundary condition variations. This straightforward explanation is to be contrasted with magnetospheric acceleration theory [Foster and Burrows, 1977] which requires a number of untested assumptions. Although we prefer solar origin as an explanation for intense polar rain, there remains an unproven possibility that spatially confined processes that undoubtedly work in the magnetosphere to produce polar cap arcs might operate on broader scales and produce the non-uniform intense precipitation. Even if the latter case is advanced, we feel that solar wind boundary conditions as outlined here remain important in determining (1) the original particle source and (2) the extent of the required particle acceleration.

8. Future Work

The access of solar electrons to the earth's polar caps produces numerous opportunities for further studies in solar and magnetospheric physics. It is, however, important to understand the degree to which field aligned potentials affect measurements in different regions. Comparisons of polar cap and magnetotail fluxes along the same field lines should be able to determine the significance of acceleration within the magnetosphere. Comparisons with interplanetary and magnetosheath data remain highly desirable in determining

the effects of bow shock and magnetopause potentials, but will have to await future instruments that are able to measure highly collimated electron distributions.

Polar rain measurements are of great potential value for solar physics. The problems of directly measuring interplanetary fluxes within one or two degrees of the magnetic field direction can be attacked by using the earth's gradually increasing field to broaden the field aligned beams to measurable widths. For instance, Foster and Burrows [1977, figure 7] measured a 4 keV intensity ratio of 1.9 between 0° and 60° at 1400 km altitude over the polar cap. Adiabatic mapping implies the same variation is present between 0° and 1° in the solar wind. This is an even more peaked distribution than our strahl model but it cannot be directly tested with existing solar wind measurements because observations in weak fields cannot begin to resolve such narrow pitch angle distributions. Such structure is, however, predicted by Olbert [1983] even when coulomb effects are considered. Interpreting such low altitude pitch angle data in this manner could yield much information on the solar origin and interplanetary propagation of such particles and contribute to the ongoing study of the problems of accelerating the high speed solar wind [Leer et al., 1982].

That part of the polar rain distribution that is determined by collisions in the lower corona contains information on coronal temperature. This is an important, but poorly known solar parameter and polar rain measurements could potentially be the best way of directly determining this quantity and the state of statistical equilibrium that exists at the coronal base.

In the magnetosphere the polar rain may well provide a clear and definitive measure of open field lines. Energetic solar electron data have been interpreted in this manner for many years [e.g. Paulikas, 1974] but such

energetic particles achieve measurable flux levels only when they are produced by large solar flares. With more continuous lower energy data one can hope to monitor the polar cap size and shape and study its variability and its relationship to regions such as boundary layers.

Acknowledgements

The authors thank C. T. Russell for allowing use of the ISEE 1 pool magnetic field data. Helpful ideas and suggestions were also provided by L. F. Burlaga.

Figure Captions

Figure 1 Schematic illustration of how interplanetary magnetic field lines connect to those of the earth. In a "toward" interplanetary sector (top) the interplanetary field lines that lead back to the sun connect to the southern tail lobe and polar cap whereas in an "away" sector (bottom) the solar connection is with the northern hemisphere. Open arrows indicate the motion of electrons coming from the sun.

Figure 2 ISEE-1 pitch angle distributions illustrating the nature of anisotropic tail lobe fluxes. The log of the distribution function is plotted versus pitch angle with every trace offset by 1.25 decades to prevent overcrowding. The instrumental one count level is indicated by a dashed line. The effective background level is slightly above the one count level especially in the sunward looking hemisphere between 90° and 150°. Meaningful counts are concentrated near the field direction at energies above 180 eV. Smooth curves represent a model solar wind distribution function mapped to the magnetotail.

Figure 3 A six hour interval of data where anisotropic lobe electrons cause $f_{\parallel}$ (lines) to be above $f_{\perp}$ (dots) at energies below 1 keV. Log f is plotted for each energy with adjacent energies offset by 1 decade to prevent overcrowding. Enhanced energetic electron fluxes after 0700 indicate entry to the plasma sheet.

Figure 4 Histograms of $f_{\parallel}/f_{\perp}$ which indicate how larger 180 eV anisotropies in the northern tail lobe are associated with away interplanetary sectors. These average f ratios are reliable indicators of the anisotropy even though they drastically underestimate the magnitude of the anisotropy (see text).

Figure 5 Contours of a model electron distribution function (light lines) constructed to represent data of Figure 2. Figure 5a represents the distribution in the solar wind and 5b illustrates the same distribution when mapped to the stronger fields of the magnetotail. A decreasing degree of anisotropy can be seen in going from the solar wind to the magnetotail; a detector sampling along the 510 eV circles in the solar wind would see f decrease by more than 6 orders of magnitude whereas in the magnetotail the decrease would be less than 3 orders of magnitude. Only electrons within the shaded region of the solar wind distribution (5a) are able to reach a tail lobe field 2.7 times larger (5b) where they form the entire distribution.

Figure 6 Two ISEE-1 lobe pitch angle distributions in the format of figure 2 are shown in the lower portion of the figure. Data are from individual spacecraft spins and the low counting rates near 90° are frequently at the one count level. The top portion of the figure shows plots of log f versus v where the 2 traces are parallel ($v_{\perp}=0$) and perpendicular ($v_{\parallel}=0$) cuts through a three dimensional surface fit to the measurements. Dots indicate one count levels. Meaningful counts are again seen only along the field direction and only the f trace in the top portion is above the 1 count level. Smooth curves in the bottom portion represent the same solar wind model mapped to two different lobe field strengths..

Figure 7 The f data from the top portion of Figure 6a are plotted on a semi-log plot vs v^2 so that straight lines indicate effective temperatures in different energy regimes. Tail lobe data above about 200 eV are generally consistent with a coronal like temperature whereas data below 200 eV are consistent with a solar wind halo temperature.

Figure 8 Solar wind plasma parameters for three published examples of intense polar rain. Low solar wind densities and or high speeds tend to be associated with the shaded regions of intense polar rain.

Figure 9 (a) Illustrating various published examples of high intensity polar cap precipitaion along with the ISEE-1 fit from Figure 7 and an example of Fennell et al. taken during dense, slow solar wind conditions. In all cases the slopes in the energy ranges <200 eV and 200-500 eV are approximately equivalent to solar wind halo and strahl temperatures respectively. (b) Indicating the energy dependence of the screening factor which determines how the 1 AU field aligned distribution function is related to the solar source distribution. Small values of the screening factor indicate that the source distribution is essentially unmodified at 1 AU whereas large values indicate that collisions and solar potential effects produce a vastly different distribution at 1 AU. High solar wind intensities (top curve) greatly enhance this modification. (c) Indicating a solar source distribution (top curve) and the portion of this distribution calculated as reaching 1 AU for the two different solar wind models used in 9b. A greater portion of the source distribution reaches 1 AU when the solar wind density is low. An effective solar "temperature" can be deduced from polar cap measurements at these times.

Figure 10 Schematic illustration of electron distribution function contours in various spatial regions in the vicinity of the earths magnetosphere.

References

Bridge, H. S., Solar cycle manifestations in the interplanetary medium, in Physics of Solar Planetary Environments, ed. by D. J. Williams, published by the American Geophysical Union, 47-62, 1976.

Burch, J. L., P. H. Reiff, J. D. Menietti, R. A. Heelis, W. B. Hanson, S. D. Shawhan, E. G. Shelley, M. Sugiura, D. R. Weimer, and J. D. Winningham, IMF By-dependent plasma flow and Birkeland currents in the dayside magnetosphere: 1. Dynamics Explorer Observations, submitted to J. Geophys. Res., 1984.

Burke, W. J., R. C. Sagalyn, M. Smiddy, M. C. Kelley, and S. T. Lai, Electric fields at high latitudes in the topside ionosphere near the dawn-dusk meridian, Space. Res., 19, 343-346, 1979.

Fairfield, D. H. and W. C. Feldman, Standing Waves at Low Mach Number Laminar Bow Shocks, J. Geophys. Res., 86, 515-522, 1975.

Feldman, W. C., J. R. Asbridge, S. J. Bame, M. D. Montgomery, and S. P. Gary, Solar wind electrons, J. Geophys. Res., 80, 4181-4196, 1975.

Feldman, W. C., J. R. Asbridge, S. J. Bame, J. T. Gosling, and D. S. Lemons, Characteristic electric variations across simple high-speed solar wind streams, J. Geophys. Res., 83, 5285-5295, 1978.

Fennell, J. F., P. F. Mizera, and D. R. Croley, Jr., Low energy polar cap electrons during quiet times, Proc. Int. Conf. Cosmic Rays, 14, MG8-3, 1267, 1975.

Fitzenreiter, R. J., A. J. Klimas, and J. D. Scudder, Detection of bump-on-tail reduced electron velocity distributions at the electron foreshock boundary, Geophys. Res. Lett., 11, 5, 496-499, 1984.

Foster, J. C. and J. R. Burrows, Electron fluxes over the polar cap, 1, Intense keV fluxes during poststorm quieting, J. Geophys. Res., 81, 6016-6028, 1976.

Foster, J. C. and J. R. Burrows, Electron fluxes over the polar cap 2. Electron trapping and energization on open field lines, J. Geophys. Res., 82, 5165-5170, 1977.

Goodrich, C. C. and J. D. Scudder, The adiabatic energy change of plasma electrons and the frame dependence of the cross-shock potential at collisionless magnetosonic shock waves, J. Geophys. Res., 89, 6654-6662, 1984.

Gussenhoven, M. S., D. A. Hardy, N. Heinemann, and R. K. Burkhardt, Morphology of the polar rain, J. Geophys. Res., in press, 1984.

Hardy, D. A., Intense fluxes of low-energy electrons at geomagnetic latitudes above 85°, J. Geophys. Res., 89, 3883-3892, 1984.

Hardy, D. A., H. K. Hills, and J. W. Freeman, Occurrence of the lobe plasma at lunar distances, J. Geophys. Res., 84, 72-78, 1979.

Heppner, J. P., Polar cap electric field distributions related to the interplanetary magnetic field direction, J. Geophys. Res., 77, 4877-4887, 1972.

Heppner, J. P., M. L. Miller, M. B. Pongratz, G. M. Smith, L. L. Smith, S. B. Mende, and N. R. Nath, The Cameo barium releases: $E_{\parallel}$ fields over the polar cap, J. Geophys. Res., 86, 3519-3542, 1981.

Holzer, T. E., Effects of rapidly diverging flow, heat addition and momentum addition in the solar and stellar wind, J. Geophys. Res., 82 23, 1977.

Jockers, K., Solar wind models based on exospheric theory, Astron. Astrophys., 6, 219, 1970.

King, J. H., Interplanetary Medium Data Book, Suppl. 1, NSSDC-WDC, 79-08, 1979.

King, J. H., Interplanetary Medium Data Book, Suppl. 2, NSSDC-WDC, 83-01, 1983.

Leer, E. and T. E. Holzer, Constraints on the solar coronal temperature in regions of open magnetic field, Solar Phys., 63, 143, 1979.

Leer, E., T. E. Holzer, and T. Flå, Acceleration of the solar wind in The source region of the solar wind, ed. by W. K. H. Schmidt and H. Grünwald, D. Reidel, Dardrecht, Holland, 1982.

Levine, R. H., M. D. Altschuler and J. W. Harvey, Solar sources of the interplanetary magnetic field and solar wind, J. Geophys. Res., 7, 1061, 1977.

Lincoln, J. V., Geomagnetic and solar data, J. Geophys. Res., 83, 1983.

Meng, C.-I. and H. W. Kroehl, Intense uniform precipitation of low energy electrons over the polar cap, J. Geophys. Res., 82, 2305-2313, 1977.

Meng, C.-I., S.-I. Akasofu, and K. A. Anderson, Dawn-dusk gradient of the precipitation of low-energy electrons over the polar cap and its relation to the interplanetary magnetic field, J. Geophys. Res., 82, 5271-5275, 1977.

Mizera, P. F. and J. F. Fennell, Satellite observations of polar, magnetotail lobe, and interplanetary electrons at low energies, Rev. Geophys. Space Physics, 16, 147-153, 1978.

Montgomery, M. D., S. J. Bame, and A. J. Hundhausen, Solar wind electrons: Vela 4 measurements, J. Geophys. Res., 73, 4999, 1968.

Munro, R. H. and B. V. Jackson, Physical properties of a polar coronal hole, Ap. J., 213, 874, 1977.

Olbert, S., Inferences about solar wind dynamics from observed distributions of electrons and ions, Proc. International School and Workshop on Plasma Astrophysics, in ESA SP-161, 135, 1981.

Olbert, S., Role of thermal conduction in the acceleration of the solar wind, in Solar Wind Five, ed. by M. Neugebauer, NASA Conference Proceedings 2280, 149-162, 1983.

Ogilvie, K. W., J. D. Scudder and H. Doong, The electron spectrometer experiment on ISEE-1, IEEE Trans. Geosci. Electronics, GS-16, 261, 1978.

Ogilvie, K. W. and J. D. Scudder, Observations of the "strahl" by the solar wind electron spectrometer on Mariner 10, in Solar Wind Four, ed. by H. Rosenbauer, Published by Max Planck Institut fur extraterrestrische Physik, Garching West Germany, 226-240, 1981.

Owocki, S. P. and J. D. Scudder, The effect of a non-maxwellian electron distribution on oxygen and iron ionization balances in the solar corona, Ap. J., 270, 758-768, 1983.

Owocki, S. P., Ph. D. thesis, University of Colorado; NCAR CT-66, Boulder, 1982.

Paulikas, G., Tracing of high-latitude magnetic field lines by solar particles, Rev. Geophys. Space Phys., 12, 117-128, 1974.

Pilipp, W. G., R. Schwenn, E. Marsch, K.-H. Muhlhauser, and H. Rosenbauer, Electron characteristics in the solar wind as deduced from Helios observations, in Solar Wind Four, ed. by H. Rosenbauer, Published by Max Planck Institut fur Aeronomie, Katlenburg-Lindau at Max Planck Institut fur extraterrestrische Physik, Garching, West Germany, 241-249, 1981.

Reiff, P. H. and D. L. Reasoner, The magnetosheath electron population at lunar distance: General Features, J. Geophys. Res., 80, 1232-1237, 1975.

Rosenbauer, H., H. Miggenrieder, M. Montgomery, and R. Schwenn, Preliminary results of the helios plasma measurements, in Physics of Solar Planetary Environments, ed. by D. J. Williams, American Geophysical Union, 319-331, 1976.

Rosenbauer, H., R. Schwenn, E. Marsch, B. Meyer, H. Miggenrieder, M. D. Montgomery, K. H. Muhlhauser, W. Pilipp, W. Voger and S. M. Zink, A survey on initial results of the Helios plasma experiment, J. Geophys., 42, 561-580, 1977.

Scudder, J. D., A. Mangeney, C. S. Wu, C. Lacombe, G. Paschmann, J. T. Gosling, C. T. Russell, R. A. Anderson, P. Rodriguez, C. Harvey, and K. W. Ogilvie, Resolution of a high β, super critical quasi-perpendicular magnetosonic shock layer, J. Geophys. Res., to be submitted, 1984.

Scudder, J. D. and S. Olbert, A theory of local and global processes which affect solar wind electrons 1. The origin of typical 1 AU velocity distribution functions - steady state theory, J. Geophys. Res., 84, 2755-2772, 1979a.

Scudder, J. D. and S. Olbert, A theory of local and global processes which affect solar wind electrons 2. Experimental Support, J. Geophys. Res., 84, 6603-6620, 1979b.

Scudder, J. D. and S. Olbert, The collapse of the local, Spitzer-Harm formulation and a global-local generalization for heat flow in an inhomogeneous, fully ionized plasma, in Solar Wind Five, NASA Conference Proceedings 2280, ed. M. Neugebauer, 163, 1983.

Schulz, M. and A. Eviatar, Electron-temperature asymmetry and the structure of the solar wind, Cosmic Electrodynamics, 2, 420- , 1972.

Sibeck, D. G. and G. L. Siscoe, Downstream properties of FTE's, submitted to J. Geophys. Res., 1984.

Sittler, E. C., Jr. and J. D. Scudder, An empirical polytrope law for solar wind thermal electrons between 0.45 and 4.76 AU: Voyager 2 and Mariner 10, J. Geophys. Res., 85, 5131, 1980.

Winningham, J., Characteristics of magnetosheath plasma observed at low altitudes in the dayside magnetospheric cusps, in Earth's Magnetospheric Processes, ed. by B. M. McCormac, D. Reidel Publishing Co., Dordrecht-Holland, 68-80, 1972.

Winningham, J. D. and W. J. Heikkila, Polar cap auroral electron fluxes observed with Isis 1, J. Geophys. Res., 79, 949-957, 1974.

Winningham, J. D. and C. Gurgiolo, DE-2 photoelectron measurements consistent with a large scale parallel electric field over the polar cap, Geophys. Res. Lett., 9. 977-979, 1982.

Yeager, D. M. and L. A. Frank, Low energy electron intensities at large distances over the earth's polar cap, J. Geophys. Res., 81, 3966-3976, 1976.

Response to Referee #2

Below are our responses to the five points raised by referee #2. The only other substantive changes involve references to a recent paper of Gussenhoven et al. and an explanation of their results via the magnetopause potential (p. 32).

1. We have made numerous corrections to the equations. The two sets of dashed lines in Figure 9a have been clarified. Figure 10 has been corrected.

2. We hope all the figures and references to them have been corrected.

3. The high energy tail in Feldman's data is at strahl energies. What was not appreciated at this time was the narrowness of the distribution. Indeed this anisotropy would produce north-south asymmetries and this had been suggested (as we stated in the introduction), but no quantitative comparisons with solar wind data had been attempted. We have inserted a sentence on p. 29 indicating that the halo-strahl distribution is convenient for modeling and describing the distribution but that there is no clear difference.

4. No attempt has been made to search for the strahl in ISEE data in the magnetosheath or interplanetary medium. It would be difficult (though not impossible) to do, but this would be a whole new study. The effects of the bow shock are discussed on page 30-31. A sentence has been added emphasizing that most polar rain particles probably traverse a distant and weak bow shock that would have little effect on the particles. Figure 10 is indeed based on the general knowledge of what the solar wind distribution function looks like.

5. Apparently no ions have been detected along with electron precipitation. The plasma sheet appears to be clearly present at lower latitudes in the Foster and Burrows data and there appears to be little question that the observations are a real polar cap phenomena. The interplanetary B_z is only slightly positive during some of this time.

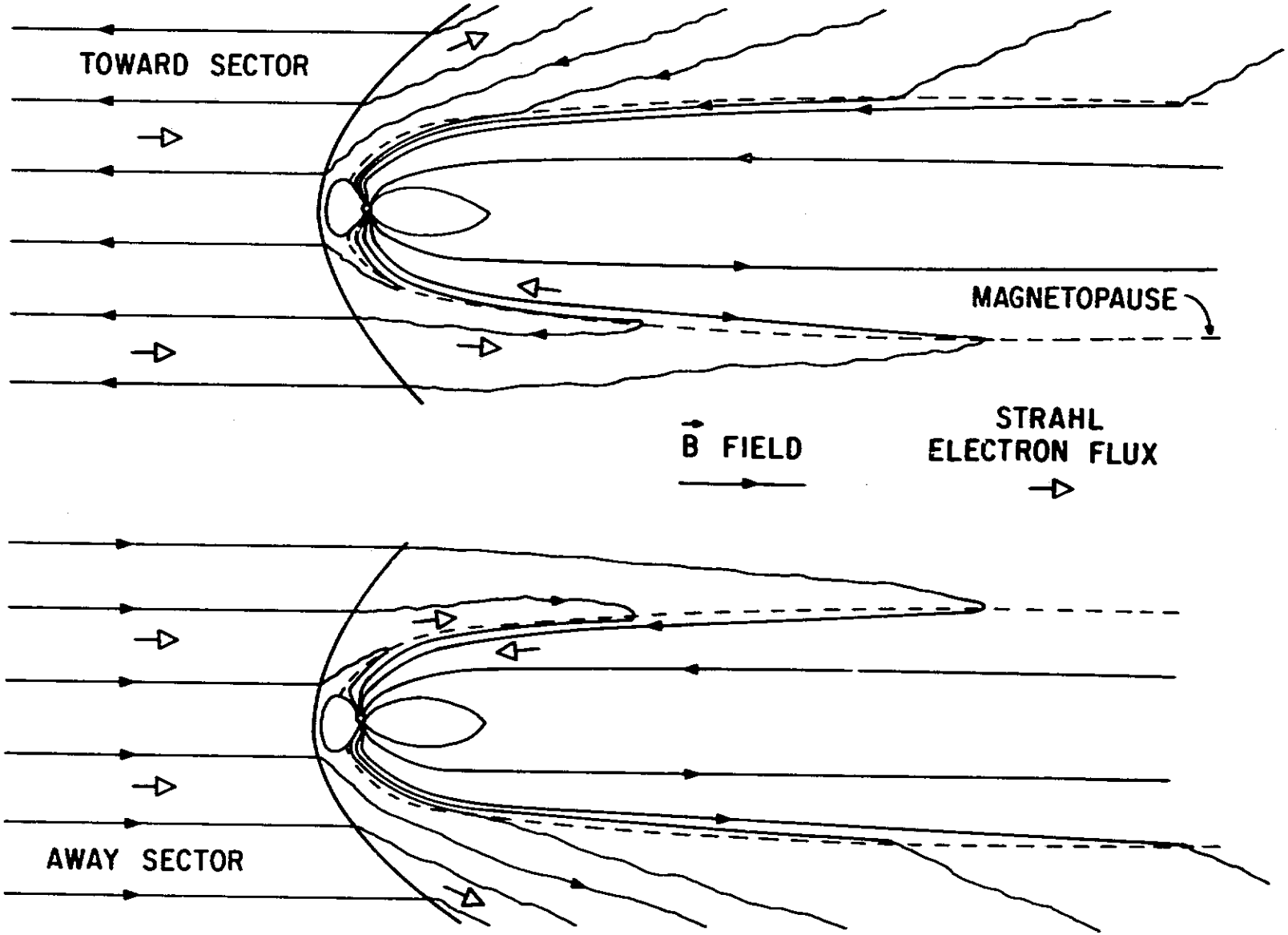
TOWARD SECTOR
MAGNETOPAUSE
B FIELD
STRAHL
ELECTRON FLUX
AWAY SECTOR

Figure 1

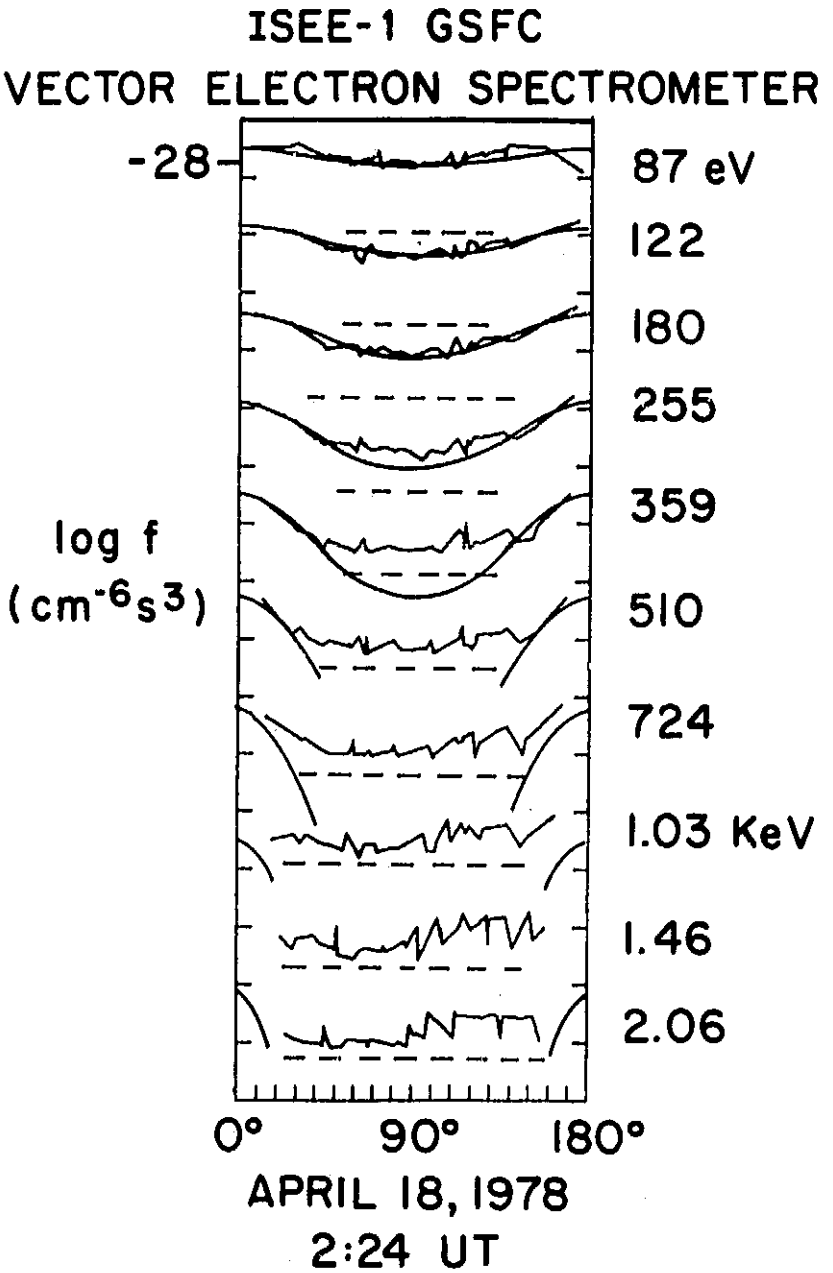
ISEE-1 GSFC
VECTOR ELECTRON SPECTROMETER
-28
log f
(cm⁻⁶s³)
87 eV
122
180
255
359
510
724
1.03 KeV
1.46
2.06
0°
90°
180°
APRIL 18, 1978
2:24 UT

Figure 2

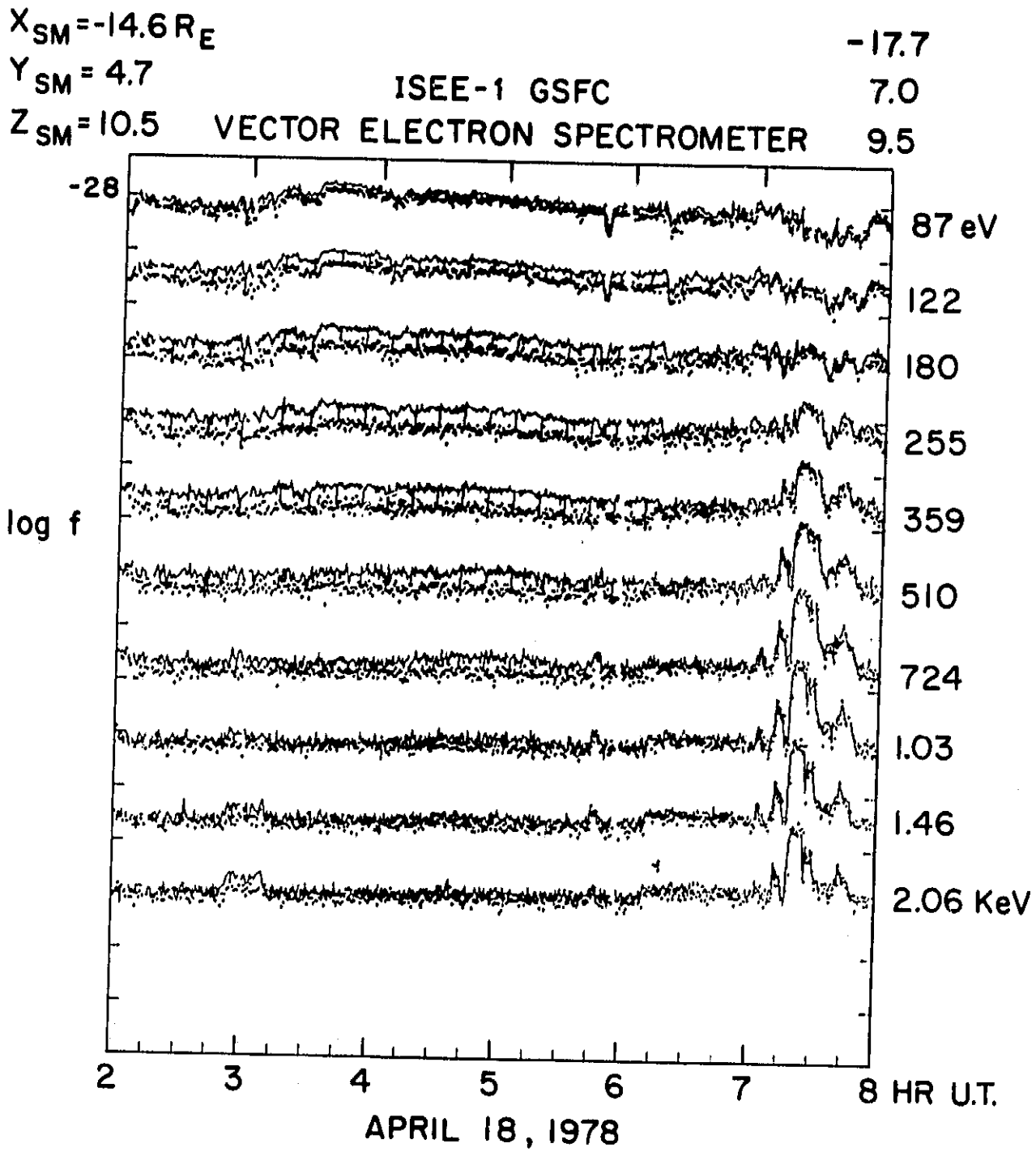
X_{SM}=-14.6 R_E
Y_{SM} = 4.7
Z_{SM}=10.5
ISEE-1 GSFC
VECTOR ELECTRON SPECTROMETER
-17.7
7.0
9.5
-28
log f
87 eV
122
180
255
359
510
724
1.03
1.46
2.06 KeV
2
3
4
5
6
7
8 HR U.T.
APRIL 18, 1978

Figure 3

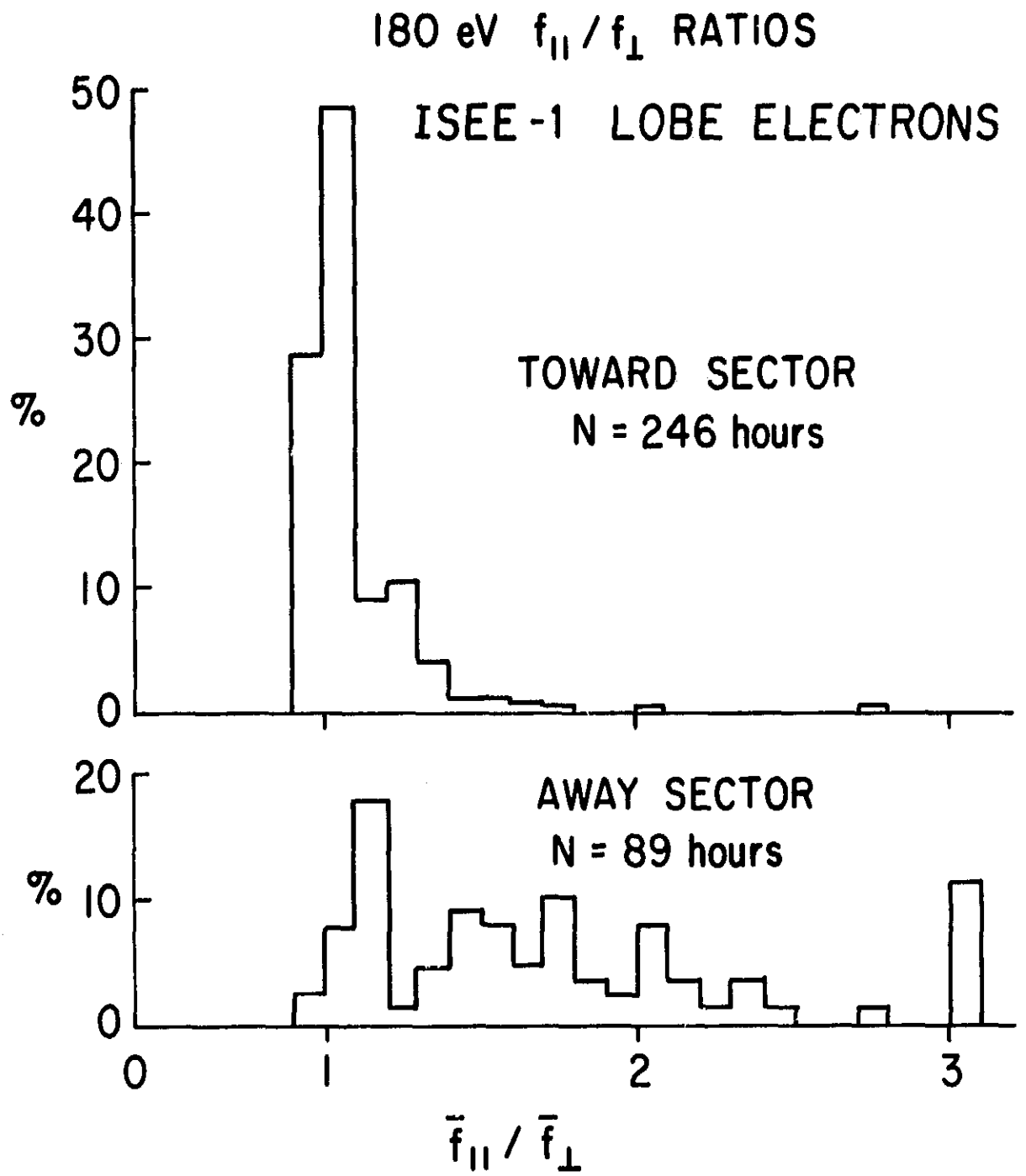
180 eV $f_{\parallel} / f_{\perp}$ RATIOS
ISEE-1 LOBE ELECTRONS
TOWARD SECTOR
N = 246 hours
AWAY SECTOR
N = 89 hours
%
50
40
30
20
10
0
20
10
0
0
1
2
3
$\bar{f}_{\parallel} / \bar{f}_{\perp}$

Figure 4

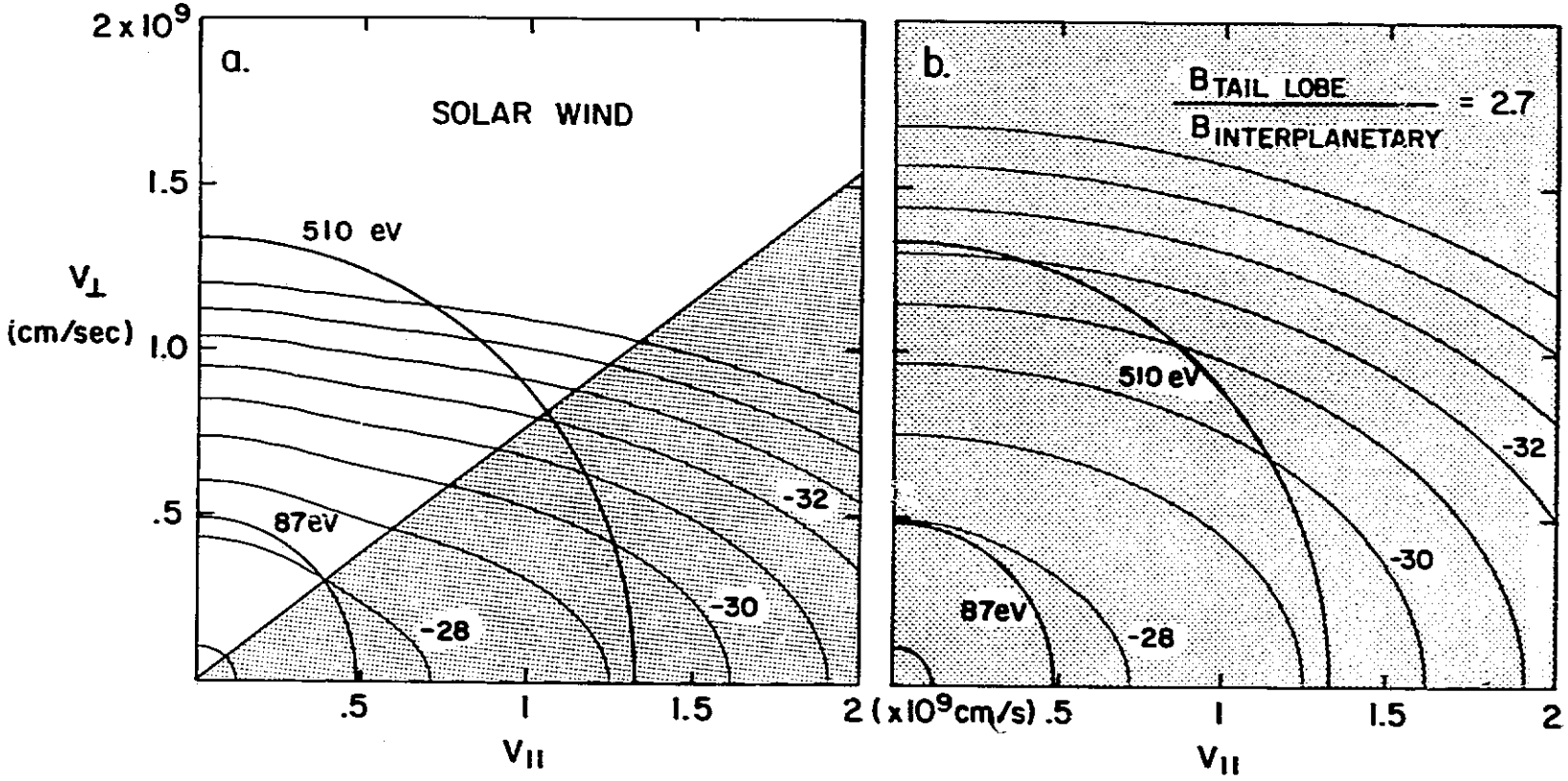
a.
SOLAR WIND
510 ev
87eV
-32
-30
-28
$V_\perp$
(cm/sec)
2×10^9
1.5
1.0
.5
.5
1
1.5
2
V_{II}
b.
$\frac{B_{TAIL\ LOBE}}{B_{INTERPLANETARY}} = 2.7$
510 eV
87eV
-32
-30
-28
(x10^{9}cm/s) .5
1
1.5
2
V_{II}

Figure 5

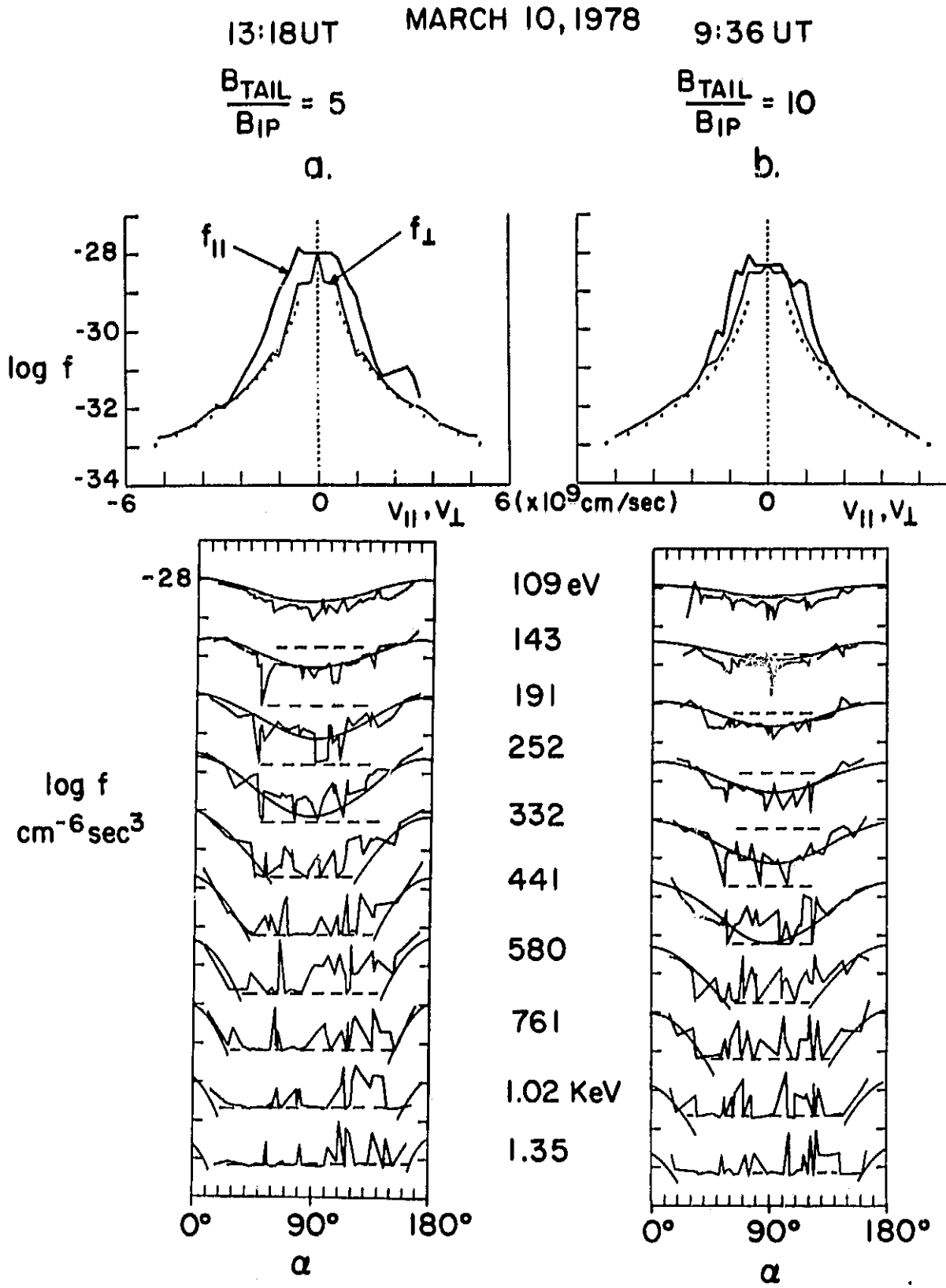
13:18UT
MARCH 10, 1978
9:36 UT
$\frac{B_{TAIL}}{B_{IP}} = 5$
$\frac{B_{TAIL}}{B_{IP}} = 10$
a.
b.
$f_{||}$
$f_{\perp}$
-28
-30
-32
-34
log f
-6
0
6
$V_{||}, V_{\perp}$
$6 (x10^9 cm/sec)$
log f
$cm^{-6} sec^3$
109 eV
143
191
252
332
441
580
761
1.02 KeV
1.35
0°
90°
180°
α

Figure 6

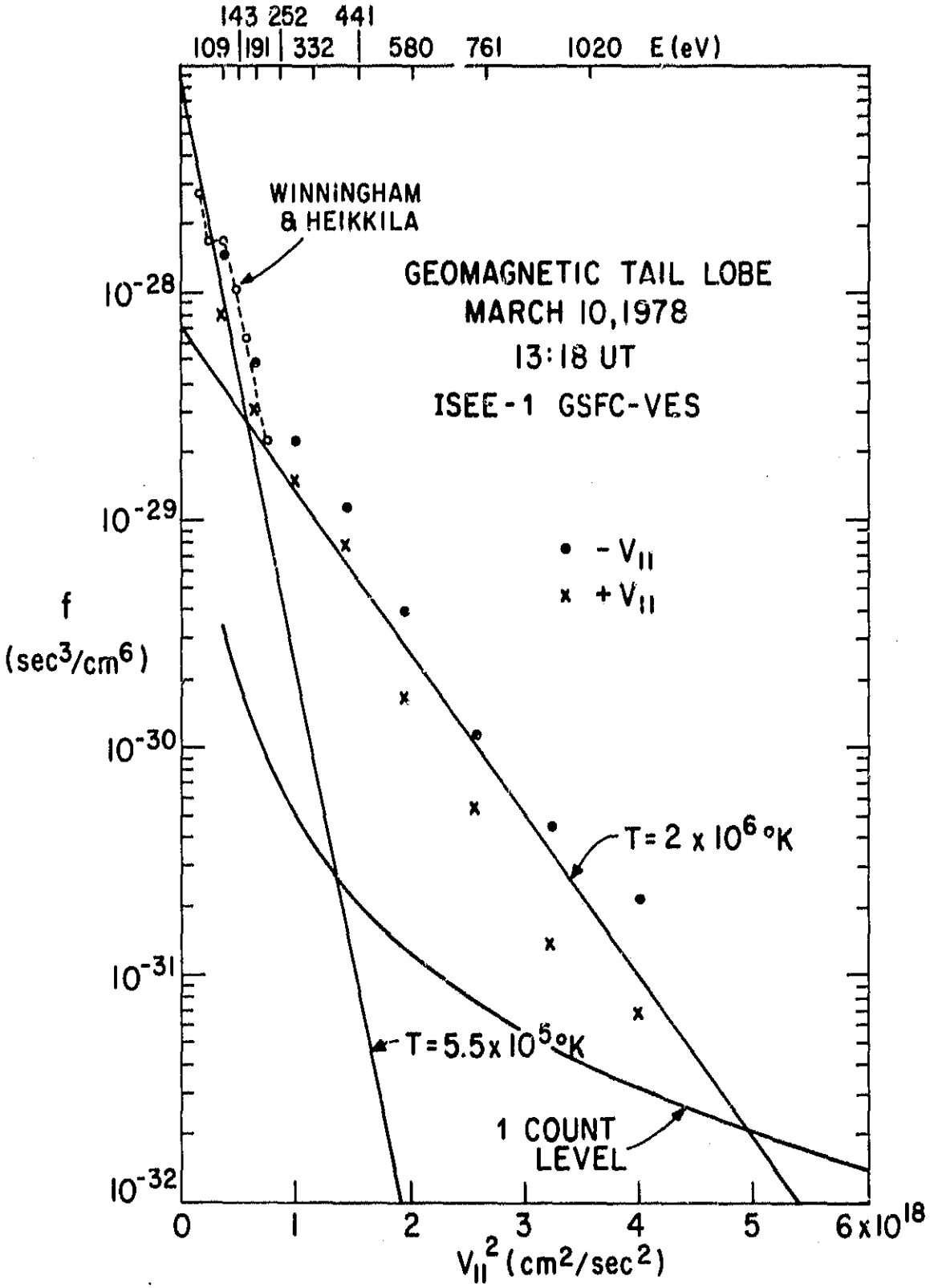
143 252 441
109 191 332 580 761 1020 E(eV)
WINNINGHAM & HEIKKILA
GEOMAGNETIC TAIL LOBE
MARCH 10, 1978
13:18 UT
ISEE-1 GSFC-VES
• - V||
x + V||
T = 2 x 10^6 °K
T = 5.5 x 10^5 °K
1 COUNT LEVEL
10^-28
10^-29
10^-30
10^-31
10^-32
f (sec^3/cm^6)
0 1 2 3 4 5 6 x 10^18
V||^2 (cm^2/sec^2)

Figure 7

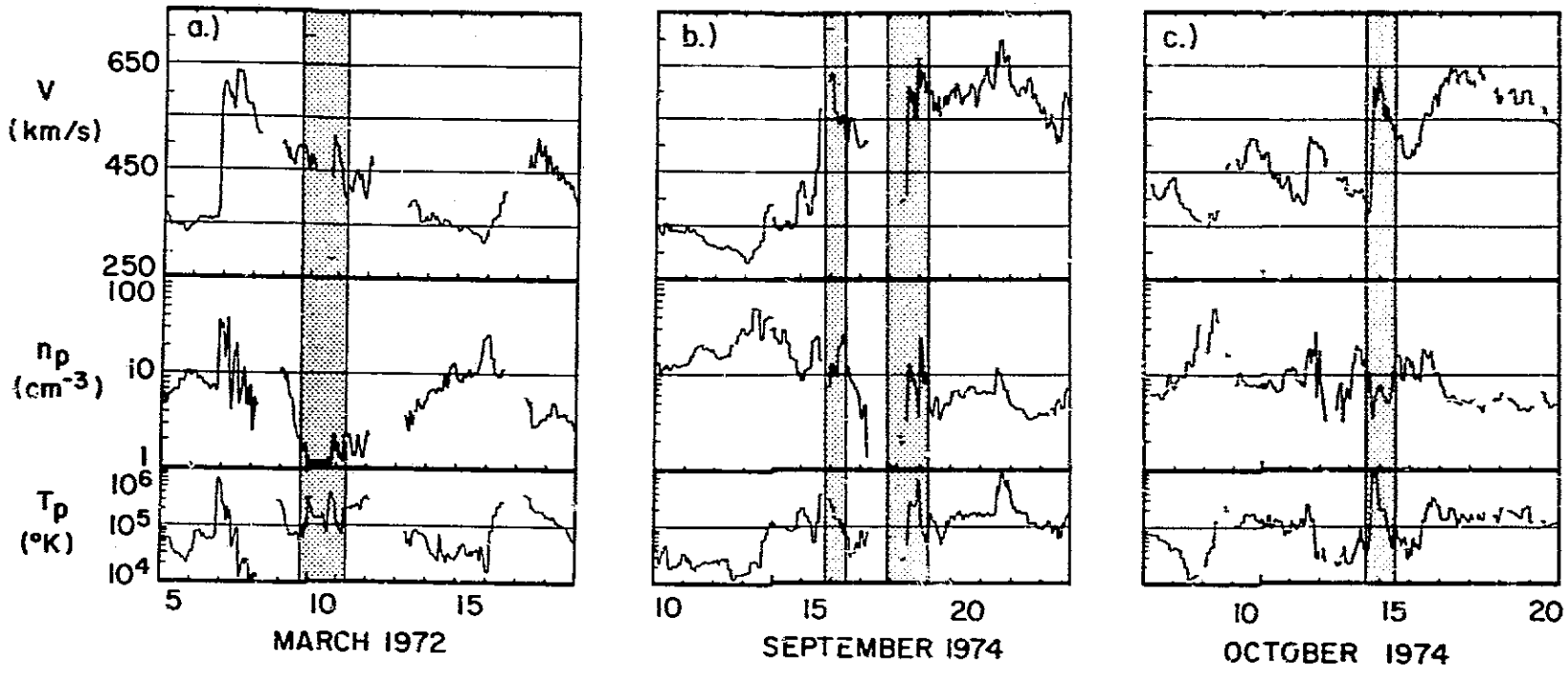
a.)
b.)
c.)
V
(km/s)
650
450
250
n_p
(cm^{-3})
100
10
1
T_p
(°K)
10^6
10^5
10^4
5
10
15
MARCH 1972
10
15
20
SEPTEMBER 1974
10
15
20
OCTOBER 1974

Figure 8

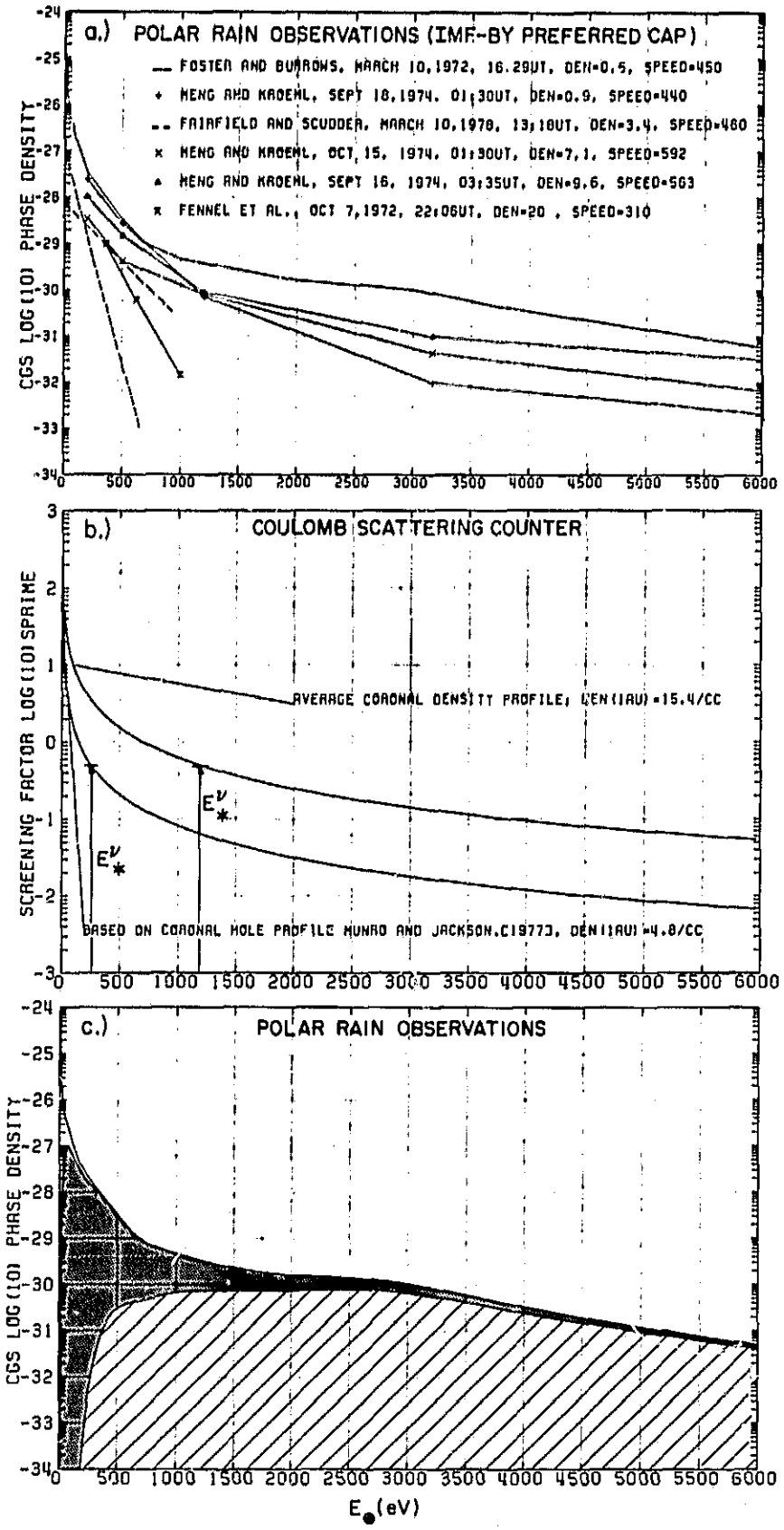
a.) POLAR RAIN OBSERVATIONS (IMF-BY PREFERRED CAP)
FOSTER AND BURROWS, MARCH 10,1972, 16.29UT, DEN=0.5, SPEED=450
HENG AND KROEHL, SEPT 18,1974, 01:30UT, DEN=0.9, SPEED=440
FAIRFIELD AND SCUDDER, MARCH 10,1970, 13:18UT, DEN=3.4, SPEED=460
HENG AND KROEHL, OCT 15, 1974, 01:30UT, DEN=7.1, SPEED=592
HENG AND KROEHL, SEPT 16, 1974, 03:35UT, DEN=9.6, SPEED=563
FENNEL ET AL., OCT 7,1972, 22:06UT, DEN=20 , SPEED=310
CGS LOG(10) PHASE DENSITY
b.) COULOMB SCATTERING COUNTER
AVERAGE CORONAL DENSITY PROFILE; DEN(1AU)=15.4/CC
BASED ON CORONAL HOLE PROFILE MUNRO AND JACKSON,C1977), DEN(1AU)=4.8/CC
SCREENING FACTOR LOG(10) SPRIME
c.) POLAR RAIN OBSERVATIONS
CGS LOG(10) PHASE DENSITY
E● (eV)

Figure 9

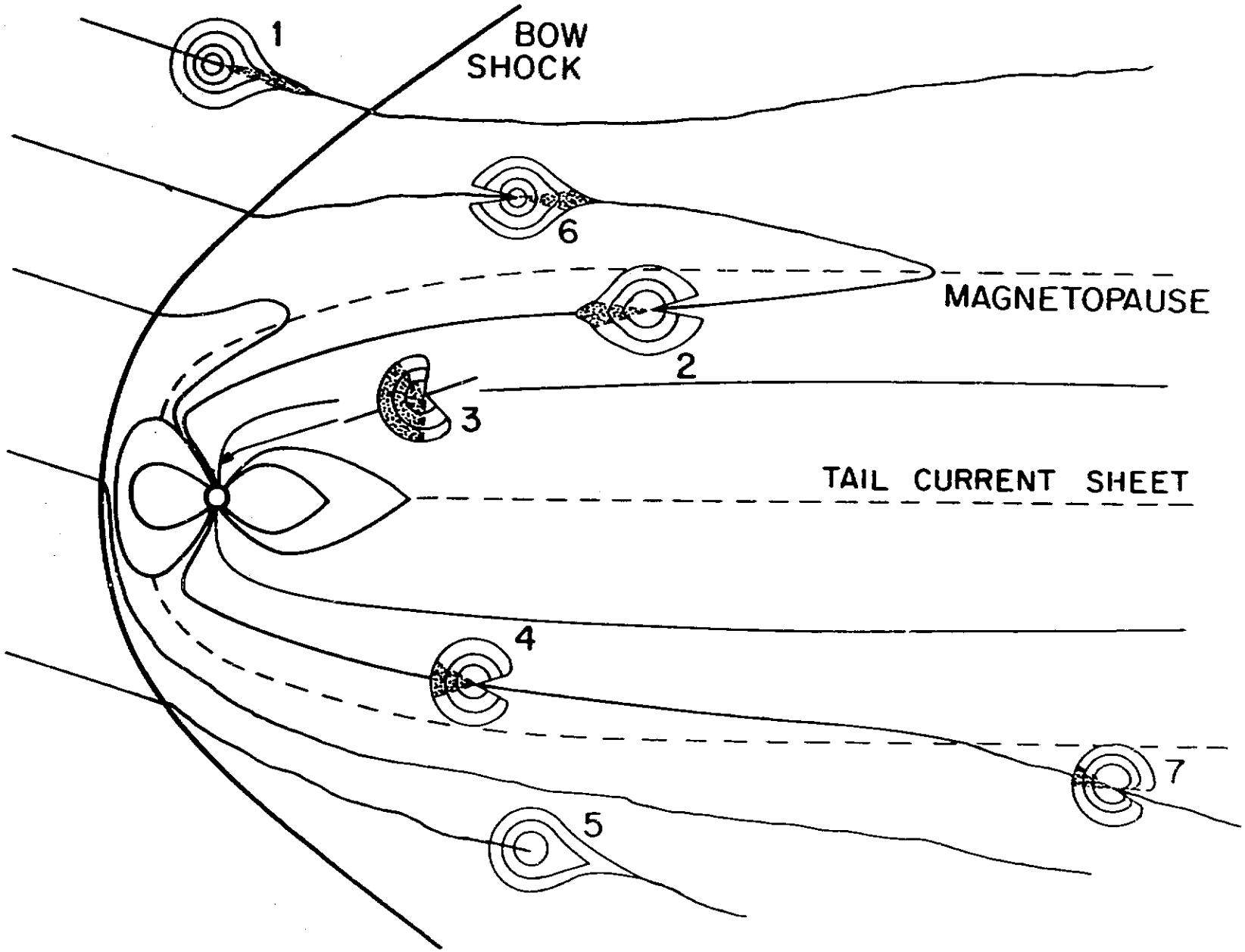

Figure 10